

1 **Early spring submarine discharge plumes fuel under-ice primary** 2 **production at a Svalbard tidewater glacier**

3

4 Tobias Reiner Vonnahme¹, Emma Persson¹, Ulrike Dietrich¹, Eva Hejdukova², Christine Dybwad¹, Josef
5 Elster³, Melissa Chierici^{4,5}, Rolf Gradinger¹

6 ¹ Department of Arctic and Marine Biology, UiT – The Arctic University of Norway, Tromsø, Norway

7 ² Department of Ecology, Faculty of Science, Charles University, Prague, Czech Republic

8 ³ University of South Bohemia, České Budějovice, and Institute of Botany ASCR, Třeboň, Czech Republic

9 ⁴ Institute of Marine Research, Tromsø, Norway

10 ⁵ University Centre in Svalbard (UNIS), Longyearbyen, Svalbard, Norway

11 *Correspondence to:* Tobias R. Vonnahme (T.r.vonnahme@gmail.com)

12 **Abstract.** Subglacial upwelling of nutrient rich bottom water is known to sustain elevated summer primary production in
13 tidewater glacier influenced fjord systems. However, during the early spring season, the importance of subglacial upwelling
14 has not been considered yet. We hypothesized that submarine discharge under sea ice is present in early spring and that its flux
15 is sufficient to increase phytoplankton primary productivity. We evaluated the effects of the submarine discharge on primary
16 production in a seasonally fast ice covered Svalbard fjord (Billefjorden) influenced by a tidewater outlet glacier in April/May
17 2019. We found clear evidence for subglacial discharge and upwelling. Although the estimated bottom water entrainment
18 factor (1.6) and total fluxes were lower than in summer studies, we still observed substantial impact on the fjord ecosystem
19 and primary production at this time of the year. The subglacial discharge leads to a salinity stratified surface layer and sea ice
20 formation with low bulk salinity and permeability. The combination of the stratified surface layer, a two-fold higher under-ice
21 irradiance due to a thinner snow cover, and higher N and Si concentrations at the glacier front supported two orders of
22 magnitude higher phytoplankton primary production ($42.6 \text{ mg C m}^{-2} \text{ d}^{-1}$) compared to a marine reference site at the fast ice
23 edge. Reciprocal transplant experiments showed that nutrient supply increased phytoplankton primary production by
24 approximately 30 %. The brackish water sea ice at the glacier front with its low bulk salinity contained a reduced brine volume,
25 limiting the inhabitable brine channel space and nutrient exchange with the underlying seawater compared to full marine sea
26 ice. Microbial and algal communities were substantially different in subglacial influenced water and sea ice compared to the
27 marine reference site, sharing taxa with the subglacial outflow water. We suggest that with climate change, the retreat of
28 tidewater glaciers in early spring could lead to decreased under-ice phytoplankton primary production. In contrast, sea ice
29 algae production and biomass may become increasingly important, unless sea ice disappears before, in which case spring
30 phytoplankton primary production may increase.

31

32

33

34 **1 Introduction**

35 Tidewater glacier fronts have recently been recognized as hotspots for marine production including top trophic levels, such as
36 marine mammals, birds and piscivorous fish (Lydersen et al., 2014, Meire et al., 2016b), but also primary producers (Meire et
37 al., 2016b., Hopwood et al., 2020). During summer, large amounts of freshwater are released below the glacier and entrap
38 nutrient rich bottom water, sediments and zooplankton during the rise to the surface (Meire et al., 2016a, Moon et al., 2018).
39 Together with katabatic winds pushing the surface water out of the fjords, submarine discharge creates a strong upwelling
40 effect (Meire et al., 2016a). The biological response to this upwelling will depend on the characteristics of the upwelled water.
41 Primary production and biomass is typically low (e.g. 0.6 ± 0.3 mg Chl *a* m⁻³, Halbach et al., 2019) in direct proximity to the
42 glacier front (within hundreds of meters to kilometres from the glacier front, Halbach et al., 2019) due to high sediment loads
43 of the plumes absorbing light, but also due to lateral advection and the time needed for algae growth (Meire et al., 2016a,b,
44 Halbach et al., 2019). The light absorbing effect of the plumes is highly dependent on the glacial bedrock type (Halbach et al.,
45 2019). The high nutrient concentrations supplied to the surface can increase summer primary production at some distance
46 (more than hundreds of meters to kilometres away from the glacier front, Halbach et al., 2019) from the initial discharge event,
47 once the sediments settled out and algae had time to grow (Meire et al., 2016, Halbach et al., 2019). These tidewater upwelling
48 effects have been described in a variety of different Arctic fjords including deep glacier termini in western Greenland (Meire
49 et al., 2016a,b), eastern Greenland (Cape et al., 2019), and north-western Greenland (Kanna et al., 2018), but also in shallower
50 fjords on Svalbard (Halbach et al., 2019). Due to the challenges of Arctic fieldwork in early spring and the difficulties of
51 locating such an outflow, only few studies investigated submarine discharge during that time window. The few studies
52 available suggest an overall low discharge flux (e.g. Fransson et al., 2020, Schaffer et al., 2020) compared to summer values.
53 However, the limited amount of data makes the generalized quantification of spring subglacial outflow difficult. In addition,
54 studies focusing on the potential impacts of the early spring discharge on both sea ice and pelagic primary production are
55 lacking.

56

57 In addition to submarine discharge at the grounding line, tidewater glacier related upwelling mechanisms can also be caused
58 by the melting of deep icebergs (Moon et al., 2018), or the melting of the glacier terminus in contact with warm seawater
59 (Moon et al., 2018, Sutherland et al., 2019). A seasonal study within an east Greenland fjord showed high melt rates of icebergs
60 throughout the year, while subglacial runoff had been detected as early as April (Moon et al., 2018). However, freshwater
61 inputs were generally substantially higher in summer (Moon et al., 2018). Glacier terminus melt rates of basal ice at the glacier-
62 marine interface are low compared to the subglacial outflow flux but can be present throughout the year (Chandler et al., 2013,
63 Moon et al., 2018). In fact, Moon et al. (2018) found higher basal iceberg melt rates below 200 m in winter compared to
64 summer. The freshwater flux from these icebergs exceeds summer river runoff and reaches values of early summer (June-July)
65 subglacial discharge (Moon et al., 2018), which may allow winter upwelling. Submarine glacier termini on Svalbard occur
66 typically at shallower water depths than on Greenland and deep basal melt at the glacier terminus (below 200 m) and iceberg

67 induced upwelling are less important (Dowdeswell, 1989). However, subglacial outflows can persist through winter and into
68 spring through the release of subglacial meltwater stored from the previous melt season (Hodgkins, 1997). Hodgkins (1997)
69 described the release of subglacial meltwater stored from the previous summer to fall melt season from various Svalbard
70 glaciers. Winter drainage occurred mostly periodically during events of ice-dam breakage in the subglacial drainage system.
71 During the storage period, the meltwater changes its chemical composition. During prolonged contact with silicon-rich
72 bedrock, the meltwater becomes enriched in the macronutrient silicate (Hodgkins, 1997). During freezing of the meltwater,
73 solutes are expelled leading to higher ion concentrations in the liquid fraction (Hodgkins, 1997). Under polythermal glaciers,
74 various other mechanisms such as constant freshwater supply from groundwater, and basal ice melt via geothermal heat,
75 pressure, or frictional dissipation can also be a continuous, but low flux meltwater source in winter and spring (Schoof et al.,
76 2014). Sediment inputs during this time of the year are low with peaks deeper in the water column, indicating limited impacts
77 on surface primary production (Moskalik et al., 2018). While studies on glacial discharge in winter and spring are limited to
78 oceanographic observations (Fransson et al., 2020, Schaffer et al., 2020), the biological effects on e.g. primary production have
79 been neglected (Chandler et al., 2013, Moon et al., 2018). We hypothesize that submarine discharge can lead to significantly
80 increased primary production, due to upwelling of nutrient-rich deeper water or through its own nutrient load, especially
81 towards the end of the spring bloom. At the same time, considerably less light absorbing sediments are entrapped due to lower
82 upwelling fluxes compared to summer (Moskalik et al., 2018). After light becomes available in spring, ice algae and
83 phytoplankton may start forming blooms fuelled by nutrients supplied via winter mixing with different onsets in different parts
84 of the Arctic. The blooms are typically terminated by limitation of macronutrients, either nitrate or silicate (Leu et al., 2015).
85 We suggest that in the absence of wind induced mixing, due to the seasonal presence of a fast ice cover in spring, submarine
86 discharge of glacial meltwater can directly (nutrient and ion enrichment over the subglacial storage period) or indirectly
87 (upwelling) be a significant source of inorganic nutrients. We suggest that these nutrients can significantly increase primary
88 production in front of tidewater glaciers compared to similar fjords without these glaciers especially after nutrients supplied
89 via winter mixing are used up (Leu et al., 2015). With climate change, these dynamics are expected to change substantially
90 (e.g. Błaszczyk et al., 2009, Holmes et al., 2019). Higher glacial melt rates and earlier runoff may initially increase tidewater
91 glacier induced upwelling, due to increased subglacial runoff (Amundson and Carroll, 2018). However, their retreat and
92 transformation into shallower tidewater glacier termini may lead to less pronounced upwelling, unless the shallower grounding
93 line is compensated by the increased runoff (Amundson and Carroll, 2018). Eventually, the tidewater glaciers transform into
94 land terminating glaciers, where wind induced mixing is still possible, but submarine discharge is eliminated (Amundson and
95 Carroll, 2018) – potentially reducing primary production.

96

97 Due to high inputs of freshwater in the autumn preceding the onset of sea ice formation, tidewater glacier influenced fjords are
98 often sea ice covered in spring, mainly by coastal fast ice. Within the sea ice, ice algae start growing, once sufficient light
99 penetrates the snow and ice layers between March and April, depending on latitude and local ice conditions (Leu et al., 2015).
100 While the beginning of the ice algal blooms is typically related to light, the magnitude depends on the initial nutrient

101 concentrations and advection of nutrient-rich seawater from the water column into the brine channel network (Gradinger,
102 2009). Thus, early spring subglacially induced upwelling has the strong potential to extend the duration and increase the
103 magnitude of the ice algal blooms. Similar control mechanisms apply to phytoplankton bloom formation and duration. Under-
104 ice phytoplankton blooms are thought to be light limited if the ice is snow covered and blooms have mostly been described in
105 areas with a lack of snow cover (e.g. melt ponds, after rain events, Fortier et al., 2002, Arrigo et al., 2014) or at the ice edge
106 related to wind-induced Ekman upwelling (Mundy et al., 2009). On Svalbard, low precipitation rates and strong katabatic
107 winds (Esau & Repina, 2012) often limit snow accumulation also on the fast ice near glacier fronts (Braaten, 1997), potentially
108 allowing enough light for under-ice phytoplankton blooms to occur. After sufficient light reaches the water column, typically
109 a diatom dominated bloom starts along the receding ice edge or even below the sea ice (e.g. Hodal et al., 2012, Lowry et al.,
110 2017). Once silicate becomes limiting for diatom growth, other taxa like *Phaeocystis pouchetii* dominate the next stage of the
111 seasonal succession (von Quillfeldt, 2000). This succession pattern can be significantly influenced by tidewater glacier induced
112 spring upwelling. Sea ice formed from brackish water has relatively low bulk salinity, low brine volume, and low total ice
113 algal biomass as observed e.g. in the Baltic Sea (Haecky & Andersson, 1999). Sea ice with reduced bulk salinity has a reduced
114 permeability compared to more saline ice at identical temperatures (Golden et al., 1998). Brackish ice conditions with low
115 algal biomass will reduce light absorption allowing more light to reach the water column potentially fuelling under-ice
116 phytoplankton blooms. We suggest that even though subglacial upwelling is diminished in the spring, compared to the summer,
117 in the absence of wind mixing, the enriched nutrient concentrations may enhance algal growth at this time of year.

118

119 We used the natural conditions in a Svalbard fjord as a model system contrasting the biological response at two glacier fronts.
120 Only one of the glacier fronts supplies submarine freshwater discharge during the winter/spring (early spring) transition period
121 while a fast ice cover was present. In contrast, the other glacier front is mostly land-terminating. The aim of the study was to
122 investigate the effect of the glacier terminus, and subglacial outflow related upwelling on the light and nutrient regime in the
123 fjord and thereby on early spring primary productivity and algae community structures both in and under the sea ice. We
124 hypothesized that; 1) submarine discharge throughout winter and spring supplies nutrient rich glacial meltwater and upwelling
125 of marine bottom water to the surface, 2) submarine discharge increases primary production near the glacier front (< 500 m),
126 3) biomass of sea ice algae is lower at glacier fronts as a result of low permeability sea ice limiting nutrient exchange and
127 inhabitable space.

128 **2 Methods**

129 **2.1 Field work and physical properties**

130 Fieldwork was conducted on Svalbard in Billefjorden (Fig. 1) between 22nd of April and 5th of May 2019, when most samples
131 were collected. For comparison, some samples had been already taken in April 2018 (seawater, sea ice, and subglacial outflow
132 water for DNA analyses) and July 2018 (glacier ice and supraglacial runoff). Billefjorden is fed by a few streams, rivers and

133 the tidewater glacier Nordenskiöldbreen and is partly fast ice covered from January to June. Nordenskiöldbreen has an
134 estimated grounding depth of 20 m at its southern margin (personal observation). Tidal currents are very slow with under 0.1
135 cm s^{-1} , which translates to advection below 22 m per tidal cycle (Kowalik et al., 2015). Katabatic winds can be strong due to
136 several glaciers and valleys leading into the fjord system (Láska et al., 2012). Together with low precipitation, this leads to a
137 thin snow depth on the sea ice. Bare sea ice spots are often present in the sea ice season (personal observations). The fjord is
138 separated from Isfjorden, a larger fjord connected to the West Spitsbergen current, by a shallow approximately 30 to 40 m sill
139 (Norwegian Polar Institute, 2020) making Billefjorden an Arctic fjord with limited impacts of Atlantic water inflows. This
140 character is shown in water masses, circulation patterns and animal communities including the presence of polar cod (Maes,
141 2017, Skogseth et al., 2020).

142 Samples were taken at three stations; 1) at the fast ice edge (IE) – a full marine reference station (78°39'09N, 16°34'01E); 2)
143 at the southern site of the ocean terminated glacier terminus (SG) (approx. 20 m water depth) with freshwater outflow observed
144 during the sampling period (78°39'03N, 16°56'44E) and; 3) at the northern site of the glacier terminus (NG) with no clear
145 freshwater outflow observed and a mostly land-terminating glacier front (78°39'40N, 16°56'19E).

146 Snow depth and sea ice thickness around the sampling area were measured with a ruler. Sea ice and glacier ice samples were
147 taken with a Mark II ice corer with an inner diameter of 9 cm (Kovacs Enterprise, Roseburg, OR, USA). Temperature of each
148 ice core was measured immediately by inserting a temperature probe (TD20, VWR, Radnor, PA, USA) into 3 mm thick pre-
149 drilled holes. For further measurements the ice cores were sectioned into the following sections: 0–3 cm, 3–10 cm and
150 thereafter in 20 cm long pieces from the bottom to the top, packed in sterile bags (Whirl-Pak™, Madison, WI, USA) and left
151 to melt at about 4–15 °C for about 24–48 h in the dark. Sections for chlorophyll *a* (Chl) measurements, DNA extractions, and
152 algae and bacteria counts were melted in 50 % vol/vol sterile filtered (0.2 μm Sterivex filter, Sigma-Aldrich, St. Louis, MO,
153 USA) seawater to avoid osmotic shock of cells (Garrison and Buck, 1986), while no seawater was added to the sections for
154 salinity and nutrient measurements. Salinity was measured immediately after melting using a conductivity sensor (YSI Pro 30,
155 YSI, USA). Brine salinity and brine volume fractions were calculated after Cox et al. (1983) for sea ice temperatures below -
156 2 °C and after Leppäranta and Manninen (1988) for sea ice temperatures above -2 °C.

157 Samples of under-ice water were taken using a pooter (Southwood and Henderson, 2000) connected to a hand-held vacuum
158 pump (PFL050010, Scientific & Chemical Supplies Ltd., UK). Deeper water at 1 m, 15 m, 25 m depths and bottom water at
159 the IE station were taken with a water sampler (Ruttner sampler, 2 L capacity, Hydro-Bios, Germany). Glacial outflow water
160 was sampled in April 2018 close to the SG station using sterile Whirl-Pak™ bags. No outflow water was found around the NG
161 station. Cryoconite hole water (avoiding any sediment) was sampled in July 2018 with a pooter on sites known to differ in
162 their biogeochemical settings (Nordenskiöldbreen main cryoconite site (NC), and Nordenskiöldbreen near Retrettøya (NR)
163 sites characterized by Vonnahme et al., 2016). One-metre long glacier surface ice samples were taken with the Mark II ice
164 corer at the southern side of the glacier on the NC site.

165 CTD profiles were taken at each station by a CastAway™ (SonTek/-Xylem, San Diego, CA, USA). At the SG station an
166 additional CTD profile was taken with a SAIV CTD SD208 (SAIV, Lakselv, Norway) including turbidity and fluorescence

167 sensors. Unfortunately, readings at the other stations failed due to sensor freezing at low air temperatures. Surface light data
168 were obtained from the photosynthetic active radiation (PAR) sensor of the ASW 1 weather station in Petuniabukta (23 m
169 a.s.l), operated by the University of South Bohemia (Láska et al., 2012, Ambrožová and Láska, 2017).
170 During the sampling days, Billefjorden was overcast. The light regime under the ice was calculated after Masicotte et al. (2018)
171 with a snow albedo of 0.78, a snow attenuation coefficient of 15 m^{-1} (Mundy et al., 2005), ice attenuation coefficients of 5.6
172 m^{-1} for the upper 15 cm and 0.6 m^{-1} below (Perovich et al., 1998). For sea ice algae, an absorption coefficient of 0.0025 m^2
173 $(\text{mg Chl})^{-1}$ was used. The fraction of fjord water vs subglacial meltwater for the water samples was calculated assuming linear
174 mixing (Equations 1-2) of the two salinities (glacial meltwater salinity = 0 PSU, average seawater salinity at IE= 34.7 ± 0.03
175 standard deviation), since no other water masses in regard to temperature or salinity signature were present (Table 1). The
176 variability of the IE seawater salinity leads to a small ($< 1\%$) uncertainty in the estimated value of the relative contributions of
177 sea water vs subglacial meltwater.

178 **2.2 Chemical properties**

179 Nutrient samples of water and melted sea ice and glacier ice were sterile filtered as described above, stored in acid washed
180 (rinsed in 5 % vol/vol HCl) and MQ rinsed 50 ml falcon tubes and kept at $-20 \text{ }^\circ\text{C}$ until processing. Total alkalinity (TA),
181 Dissolved inorganic carbon (DIC), and pH samples were sampled in 500 ml borosilicate glass bottles avoiding air
182 contamination and fixed within 24 h with 2 % (final conc.) HgCl_2 and stored at $4 \text{ }^\circ\text{C}$ until processing.

183 Nutrients were measured in triplicates using standard colorimetric methods with a nutrient autoanalyser (QuAAtro 39, SEAL
184 Analytical, Germany) using the instrument protocols: Q-068-05 Rev. 12 for nitrate (detection limit = $0.02 \text{ } \mu\text{mol L}^{-1}$), Q-068-
185 05 Rev. 12 for nitrite (detection limit = $0.02 \text{ } \mu\text{mol L}^{-1}$), Q-066-05 Rev. 5 for silicate (detection limit = $0.07 \text{ } \mu\text{mol L}^{-1}$), and Q-
186 064-05 Rev. 8 for phosphate (detection limit = $0.01 \text{ } \mu\text{mol L}^{-1}$). The data were analysed using the software AACE v5.48.3
187 (SEAL Analytical, Germany). Reference seawater (Ocean Scientific International Ltd., United Kingdom) was used as blanks
188 for calibrating the nutrient analyser. The maximum differences between the measured triplicates were $0.1 \text{ } \mu\text{mol L}^{-1}$ for silicate
189 and nitrate and $0.05 \text{ } \mu\text{mol L}^{-1}$ for nitrite and phosphate. Concentrations of nitrate and nitrite (NO_x) were used to estimate the
190 fraction of bottom water reaching the surface at SG assuming linear mixing of subglacial meltwater, bottom water (at station
191 IE) and surface water concentration using the NO_x concentration measured at IE and the subglacial meltwater (Table 1). The
192 calculations for these mixing estimates are given in the appendix (Equations 3-6).

193 DIC and TA were analyzed within 6 months after sampling as described by Jones et al. (2019) and Dickson et al. (2007). DIC
194 was measured on a Versatile Instrument for the Determination of Titration carbonate (VINDTA 3C, Marianda, Germany),
195 following acidification, gas extraction, coulometric titration, and photometry. TA was measured with potentiometric titrations
196 in a closed cell on VINDTA Versatile INstrument for the Determination of Titration Alkalinity, VINDTA 3S, Marianda,
197 Germany). Precision and accuracy was ensured via measurements of Certified Reference Materials (CRM, obtained from
198 Dickson, Scripps Institution of Oceanography, USA). Triplicate analyses on CRM samples showed mean standard deviations
199 below $\pm 1 \text{ } \mu\text{mol kg}^{-1}$ for DIC and TA.

200 **2.3 Biomass and communities**

201 For determination of algal pigment concentrations, about 500 ml sea water or melted sea ice were filtered onto GF/F filter
202 (Whatman plc, Maidstone, UK) in triplicates using a vacuum pump (max 200 mbar vacuum) before storing the filter in the
203 dark at -20 °C. Water and melted sea ice for DNA samples were filtered onto Sterivex filter (0.2 µm pore size) using a peristaltic
204 pump and stored at -20 °C until extraction. Algae were sampled in two ways; 1) a phytoplankton net (10 µm mesh size) was
205 pulled up from 25 m and the samples fixed in 2 % (final conc.) neutral Lugol and stored at 4 °C in brown borosilicate glass
206 bottles before processing; and 2) water or melted sea ice was fixed and stored directly as described above. For later bacteria
207 abundance estimation, 25 ml of water was fixed with 2 % (final conc.) formaldehyde for 24–48 h at 4 °C before filtering onto
208 0.2 µm polycarbonate filters (Isopore™, Merck, US) and washing with filtered seawater and 100 % ethanol before freezing at
209 -20 °C.

210 Algal pigments (Chl *a*, phaeophytin) were extracted in 5 ml 96 % ethanol at 4 °C for 24 h in the dark. The extracts were
211 measured on a Turner Trilogy AU-10 fluorometer (Turner Designs, 2019) before and after acidification with a drop of 5 %
212 HCl. 96 % ethanol was used as a blank and the fluorometer was calibrated using a chlorophyll standard (Sigma S6144). For
213 estimations of algae derived carbon, a conversion factor of 30 g C (g Chl)⁻¹ was applied (Cloern et al., 1995). The maximum
214 differences (max-min) between the measured triplicates were under 0.05 µg Chl L⁻¹ unless stated otherwise.

215 DNA was isolated from the Sterivex filter cut out of the cartridge using sterile pliers and scalpels, using the DNeasy®
216 PowerSoil® Kit following the kit instructions with a few modifications. Solution C1 was replaced with 600 µL
217 Phenol:Chloroform:Isoamyl Alcohol 25:24:1 and washing with C2 and C3 was replaced with two washing steps using 850 µL
218 chloroform. Before the last centrifugation step, the column was incubated at 55 °C for 5 min to increase the yield. For microbial
219 community composition analysis, we amplified the V4 region of a ca. 292 bp fragment of the 16S rRNA gene using the primers
220 (515F, GTGCCAGCMGCCGCGGTAA and 806R, GGACTACHVGGGTWTCTAAT, assessed by Parada et al., 2016). For
221 eukaryotic community composition analyses, we amplified the V7 region of ca 100-110 bp fragments of the 18S rRNA gene
222 using the primers (Forward 5'-TTTGTCTGSTTAATTSCG-3' and Reverse 5'-GCAATAACAGGTCTGTG-3', assessed by
223 Guardiola et al., 2015). The Illumina MiSeq PE library was prepared after Wangenstein et al. (2018).

224 For qualitative counting of algal communities, the phytoplankton net and bottom sea-ice samples were counted under an
225 inverted microscope (Zeiss Primovert, Carl Zeiss AG, Germany) with 10x40 magnification. For quantitative counts, 10-50 ml
226 of the fixed water samples were settled in an Utermöhl chamber (Utermöhl, 1958) and counted. Algae were identified using
227 identification literature by Tomas (1997), and Throndsen et al. (2007). For bacteria abundance estimates, bacteria on
228 polycarbonate filter samples were stained with DAPI (4,6-diamidino-2-phenylindole) as described by Porter and Feig (1980),
229 incubating the filter in 30 µl DAPI (1 µg ml⁻¹) for 5 min in the dark before washing with MQ and ethanol and embedding in
230 Citifluor:Vectashield (4:1) onto a microscopic slide. The stained bacteria were counted using an epifluorescence microscope
231 (Leica DM LB2, Leica Microsystems, Germany) under UV light at 10x100 magnification. At least 10 grids or 200 cells were
232 counted. The community structure of the phytoplankton net haul was used for estimating the contribution of sea ice algae to

233 the settling community based on typical Arctic phytoplankton (Von Quillfeldt, 2000) and sea ice algal species (von Quillfeldt
234 et al., 2003) described in literature.

235 **2.4 In situ measurements and incubations**

236 Vertical algal pigment fluxes were measured using custom made (Faculty of Science, Charles University, Prague, Czech
237 Republic) short-term sediment traps (6.2 cm inner diameter, 44.5 cm height) at 1 m, 15 m, and 25 m under the sea ice anchored
238 to the ice at SG and IE, as described by Wiedmann et al. (2016). Sediment traps were left for 24 h at the SG station and 37 h
239 at the IE station. After recovery, samples for algal pigments were taken, fixed and analysed as described above. Vertical export
240 fluxes were calculated as described in equation 7.

241 Primary production (PP) was measured based on ^{14}C -DIC incorporation. Samples were incubated *in situ* in 100 ml polyethylene
242 bottles attached to the rig of the sediment trap giving identical incubation times. Seawater or bottom sea ice melted in filtered
243 seawater (ca 20 °C initial temperature to ensure fast ice melt) on site were incubated with ^{14}C sodium bicarbonate at final
244 concentration of $1 \mu\text{Ci ml}^{-1}$ (PerkinElmer Inc., Waltham, USA). PP samples were incubated in triplicates for each treatment
245 with two dark controls for the same times as the sediment traps. Samples were filtered onto precombusted Whatman GF/F
246 filters (max 200 mbar vacuum) and acidified with a drop of 37 % fuming HCl for 24 h for removing remaining inorganic
247 carbon. The samples were measured in the Ultima Gold™ Scintillation cocktail on a liquid scintillation counter (PerkinElmer
248 Inc., Waltham, USA, Tri-Carb 2900TR) and PP was calculated after Parsons et al. (1984). Dark carbon fixation (DCF) rates
249 were used to estimate bacterial biomass production using a conversion factor of $190 \text{ mol POC (mol CO}_2\text{)}^{-1}$ fixed (Molari et al.,
250 2013).

251 For testing the effect of the water chemistry on phytoplankton growth, we designed a reciprocal transplant experiment where
252 the phytoplankton communities at SG and IE (1 m and 15 m) were transplanted into the sterile filtered water of both SG and
253 IE. 50 ml of the water containing the phytoplankton communities of SG or IE were transferred into 50 ml sterile filtered (0.2
254 μm) seawater of SG or IE in 100 ml polyethylene bottles. The bottles with IE communities were then incubated under the ice
255 at the IE station and the SG communities under the ice at the SG station. The aim of the experiment is to test if water chemistry
256 alone is sufficient to increase primary production, or if the different communities, light regimes, or temperatures are more
257 important. These samples were incubated and processed together with the other PP incubations at the respective depths as
258 described above.

259 **2.5 Statistics and bioinformatics**

260 Silicate, phosphate and NO_x concentrations were plotted against salinities and tested for correlations via linear regression
261 analysis using the lm function in R (R Core Team, Vienna, Austria). P values were corrected for multiple testing using the
262 false discovery rate. Since the primary production estimates of the reciprocal transplant experiments were not normally
263 distributed, came from a nested design, and had heterogeneous variance, a robust nested Analysis of variance (ANOVA) was
264 performed to test for significant treatment effects of incubation water with water depth as nested variable. The map (Fig. 1)

265 was created in R using the PlotSvalbard v0.9.2 package (Vihtakari, 2020). The Svalbard basemap was retrieved from the
266 Norwegian Polar institute (2020, CC BY 4.0 license), the pan-Arctic map was retrieved from Natural Earth (2020, CC Public
267 domain license), and the bathymetric map was retrieved from the Norwegian mapping authority (Kartverket, 2020, CC BY 4.0
268 license).

269 16S sequences were analysed using a pipeline modified after Atienza et al. (2020) based on OBITools v1.01.22 (Boyer et al.,
270 2014). The raw reads were demultiplexed and trimmed to a median phred quality score minimum of 40 and sequence lengths
271 between 215 bp and 299 bp (16S rRNA) or between 90 bp and 150 bp (18S rRNA) and merged. Chimaeras were removed
272 using uchime with a minimum score of 0.9. The remaining merged sequences were clustered using swarm (Mahe et al., 2014).
273 16S swarms were classified using the RDP classifier (Wang et al., 2007) and 18S swarms using the sina aligner (Pruesse et
274 al., 2012) with the silva SSU 138.1 database (Quast et al., 2012). Further multivariate analyses were done in R using the vegan
275 package. The non-metric multidimensional scaling (NMDS) plots are based on Bray-Curtis dissimilarities of square root
276 transformed and double Wisconsin standardized OTU tables and were used to visualize differences between groups (brackish
277 water at SG – Fjord water, sea ice – seawater). Analysis of Similarities (ANOSIM) were done to test for differences of the
278 communities between the groups (999 permutations, Bray-Curtis dissimilarities).

279 **3 Results**

280 **3.1 Physical parameters**

281 The physical conditions of sea ice (temperature T/bulk salinity S, Fig. 2a,b) and surface water (uppermost 4 m under the sea
282 ice, T and S, Fig. 2c,d) at the freshwater inflow impacted site SG differed substantially from NG and IE. The sea ice and the
283 upper 4 m under the sea ice had consistently lower salinities (<8 PSU) and higher temperatures (-0.4 °C to -0.2 °C) at SG
284 compared to NG and IE and also compared to the deeper water masses at SG (salinity > 34.6 PSU, temperature < -1.4 °C)(Fig.
285 2c,d). Sea ice melt was unlikely because the measured water temperatures and sea ice temperatures were below the freezing
286 point considering the sea ice bulk salinity. The water column at SG was highly stratified with a low salinity 4 m thick layer
287 under the sea ice, separated by a sharp ca 1 m thick pycnocline (Fig. 2c,d). In contrast, the water column at IE was fully mixed
288 and at NG only a minor salinity drop from 34.6 to 33.6 PSU occurred within the the upper 50 cm under the sea ice (Fig. 2c,d).
289 Sea ice temperature and salinity showed similar variations between the three sites with SG ice having lower salinities and
290 higher temperatures relative to sea ice at the other stations (Fig. 2a,b). At SG, bulk salinities were mostly below 0.7 PSU and
291 calculated brine salinities below 14 PSU, except for the uppermost 20 cm where bulk salinities reached around 1.7 PSU and a
292 brine salinity of 32 PSU (Fig. 2). This resulted in very low brine volume fractions below 5 %, except for the lowermost 10 cm
293 with brine volume fractions up to 9 % (Supplementary table S1). At IE and NG, bulk salinities are mostly above 5 PSU (>40
294 PSU brine salinity) and temperatures were below -0.4 °C, which led to brine volume fractions above 6 % in all samples and
295 above 10 % in the bottom 30 cm.

296 The homogenous temperature and salinity water column profiles at IE and NG stations indicate the presence of only one water
297 mass (Local Arctic water, Skogseth et al., 2020). The only additional water mass was subglacial meltwater (salinity of 0 PSU)
298 mixed into the surface layer of SG. Applying a simple mixing model based on the two salinities (IE= 34.7 PSU, Glacier= 0
299 PSU) provided an estimation of the fraction of glacially derived water in the surface layer of ca. 85 % in the uppermost 2 m
300 under the sea ice, before decreasing to 0 % at 4 m under the sea ice below the strong halocline. The water sample taken 1 m
301 under the sea ice had a fraction of 32 % glacial meltwater (Table 1). For NG, glacial derived water contributed only 3 % in the
302 first 50 cm under the sea ice.

303 The SG station was 33 m deep and about 180 m away from the glacier front. The sea ice was 1.33 m thick and covered by 3
304 cm of snow. The ice appeared clear with some minor sediment and air bubble inclusions and missed a skeletal bottom layer.
305 In the water column, a higher potential sediment load was observed as a turbidity peak at the halocline (Fig. 3). Direct evidence
306 of subglacial outflow had been observed at the southern site of the glacier in form of icing and liquid water flowing onto the
307 sea ice in April 2018, April 2019 and October 2019 (Fig. S4), but this form of subglacial outflow froze before reaching the
308 fjord, which was additionally blocked by impermeable sea ice. The sea ice temperature was between -0.4 °C at the bottom and
309 -1.7 °C at the top (Fig. 2b).

310 NG was 27 m deep and about 360 m away from the glacier front. The sea ice was thinner (0.92 m) and the snow cover thicker
311 (6 cm) compared to SG. The ice had a well developed skeletal layer at the bottom with brown coloration due to algal biomass.
312 The ice temperature ranged between -2 °C at the bottom to -2.7 °C at the top (Fig. 2b). The IE station was about 75 m deep
313 and 50 m away from the ice edge. The sea ice was thinnest (0.79 m) and the snow cover thickest (10 cm). Sea ice temperatures
314 were coldest ranging from -2.2 °C at the bottom to -3.1 °C on the top (Fig. 2b). Loosely floating ice algae aggregates were
315 present in the water directly under the ice. The recorded surface PAR irradiance were similar during the primary production
316 incubation times at SG and IE (SG: average=305 $\mu\text{E m}^{-2} \text{s}^{-1}$, min=13 $\mu\text{E m}^{-2} \text{s}^{-1}$, max=789 $\mu\text{E m}^{-2} \text{s}^{-1}$; IE: average=341 $\mu\text{E m}^{-2}$
317 s^{-1} , min=37 $\mu\text{E m}^{-2} \text{s}^{-1}$, max=909 $\mu\text{E m}^{-2} \text{s}^{-1}$). Using published attenuation coefficients irradiance directly under the ice was 5
318 $\mu\text{E m}^{-2} \text{s}^{-1}$ at IE and with 9 $\mu\text{E m}^{-2} \text{s}^{-1}$ higher at SG due to the thinner snow cover.

319 **3.2 Nutrient variability in sea ice and water**

320 Subglacial outflow water and glacial ice had relatively low nutrient levels (in glacial ice: $\text{Si(OH)}_4 < 0.3 \mu\text{mol L}^{-1}$, $\text{NO}_x < 0.9$
321 $\mu\text{mol L}^{-1}$, $\text{PO}_4 < 0.75 \mu\text{mol L}^{-1}$, in outflow: $\text{Si(OH)}_4 < 1.5\text{-}2.0 \mu\text{mol L}^{-1}$, $\text{NO}_x 1.8\text{-}2.3 \mu\text{mol L}^{-1}$, $\text{PO}_4 < 0.1 \mu\text{mol L}^{-1}$), but the
322 nutrient concentrations in subglacial outflow water were higher than in most sea ice samples and the depleted surface water (1
323 m under the sea ice) at the IE. Nutrient concentrations in the fjord were highest in the bottom water (4.0- 4.5 $\mu\text{mol L}^{-1}$ Si(OH)_4 ,
324 9.1- 9.6 $\mu\text{mol L}^{-1}$ NO_x , 0.7-0.8 $\mu\text{mol L}^{-1}$ PO_4) and depleted at the surface and in the sea ice with the exception of the under-
325 ice water (UIW, 0- 1 cm under the sea ice) of SG, where NO_x (10 $\mu\text{mol L}^{-1}$) and silicate (19 $\mu\text{mol L}^{-1}$) levels were exceptionally
326 high (Fig. 4). We cannot exclude anomalies or sampling artifacts to be responsible for the high UIW values, and therefore used
327 the values measured 1 m under the sea ice for further calculations in this manuscript as surface water reference. SG had overall
328 higher levels of silicate and NO_x compared to the IE at both 1 m below the sea ice (factors of 3 for Si(OH)_4 and 2 for NO_x)

329 and bottom ice (factor of 18 for $\text{Si}(\text{OH})_4$ and 3 for NO_x compared to IE bottom ice) (Fig. 4). Silicate concentrations deeper in
330 the water column were similar at all the stations with values of ca $4 \mu\text{mol L}^{-1}$. Close to the surface silicate was reduced to 1.6
331 $\mu\text{mol L}^{-1}$ at 1 m at the IE, while it stayed at $4.3 \mu\text{mol L}^{-1}$ at SG (Fig. 4a). In the water column, NO_x and phosphate gradients
332 were similar between the sites. However in sea ice, NO_x concentrations were more than two times higher at SG than at the IE.
333 In the bottom 30 cm of sea ice all nutrients had higher concentrations at SG, except for phosphate, which was depleted in the
334 bottom 3 cm of SG, but not in the bottom of IE sea ice. In the ice interior at 50- 70 cm distance from the ice bottom, also the
335 other nutrients were depleted at SG, before rising slightly towards the surface of the ice. N:P ratios were generally highest at
336 SG with values above 40, exceeding Redfield ratios in the surface water and sea ice. N:P ratios at the IE were below Redfield
337 in the entire water column and bottom sea ice with values ranging from 10 to 13. A slight increase in NO_x was observed at the
338 sea ice-atmosphere interface at NG and SG.

339 Nutrient versus salinity profiles can give indications of the endmembers (sources) of the nutrients (Fig. 5) with a linear
340 correlation being indicative of conservative mixing. A positive correlation indicates higher concentrations of the nutrients of
341 the saline Atlantic water endmember, while a negative correlation points to a higher concentration in the fresh glacial meltwater
342 endmember. Biological uptake and remineralisation could weaken or eliminate the correlation, indicating non-conservative
343 mixing. In the water column at NG and IE silicate ($R^2=0.66$, $p=0.008$), NO_x ($R^2=0.62$, $p=0.01$) and phosphate ($R^2=0.69$,
344 $p=0.005$) showed conservative positive mixing patterns with higher contributions of Atlantic water (Fig. 5a-c). SG showed a
345 negative correlation for silicate pointing to a higher contribution of glacial meltwater ($R^2=0.86$, $p<0.0001$). The absence of
346 correlations for NO_x and PO_4 indicate non-conservative mixing pointing towards the relevance of biological uptake and release
347 (Fig. 5d-f). At SG, silicate concentrations were higher with lower salinities. The same pattern was observed in sea ice, with
348 higher silicate and NO_x concentrations in the fresher SG ice, compared to NG and IE (Fig. 5g-i). However, the R^2 value were
349 lower in particular for $\text{Si}(\text{OH})_4$ (NO_x : $R^2=0.18$, $p=0.059$; $\text{Si}(\text{OH})_4$: $R^2=0.41$, $p=0.002$).

350 The contribution of nutrients by upwelling as well as freshwater inflow from glacial meltwater at SG was estimated by linear
351 mixing calculations for 1 m below the sea ice, avoiding the potential outlier values directly under the ice (Equations 1-6). At
352 1 m below the sea ice, about 32 ± 0.1 % of the water was derived from glacial meltwater based on salinity-based mixing of
353 glacial meltwater and local Arctic water (Table 1, Eq. 1-2). The remaining 68 % came from either bottom water upwelling (25
354 m at SG as reference) or surface water (IE values at 1 m under the sea ice as reference). Inorganic nutrients behaved
355 conservatively at the IE reference (Fig. 5a-c), which allows similar mixing calculation of the bottom water fraction. Based on
356 linear mixing of inorganic nutrients, 58 ± 1 % of NO_x and 49 ± 3 % of PO_4 was provided by subglacial upwelling (Table 1).
357 For silicate, higher concentrations were required in the bottom water of subglacial meltwater at the glacier front to explain the
358 very high surface concentrations measured. Considering the estimated NO_x and PO_4 fractions, the overall fraction of nutrients
359 derived from upwelling was about 53 %. The overall budget 1 m under the sea ice is was 32 ± 0.1 % glacial meltwater, 53 ± 3
360 % subglacial upwelling (marine bottom water), and 15 ± 3 % horizontal transport (surface water).

361 3.3 Carbon cycle

362 Net primary productivity (NPP) was overall one order of magnitude higher at SG than at IE, with the highest production value
363 occurring within the brackish layer under the ice at SG ($5.27 \text{ mg m}^{-3} \text{ d}^{-1}$, Fig. 6, 7). Within this layer, also Chl values were
364 about two times higher compared to IE (21 mg m^{-3} at SG, 9.1 mg m^{-3} at IE), and also the Chl-specific productivity in this layer
365 exceeded values at the other stations (Table 2). Within sea ice, a slightly different pattern emerged. While the primary
366 productivity in the bottom sea ice (0–3 cm) was two times higher at SG compared to IE, Chl values were two order of
367 magnitudes lower (Fig. 6). This indicates high Chl-specific production at SG ($5.6 \text{ mg C mg Chl d}^{-1}$ in the sea ice and 11.4 mg
368 C mg Chl d^{-1} integrated over 25 m depth). At the IE, the contribution of released ice algae to algal biomass in the water column
369 was higher and the overall vertical Chl flux was about 1.5 times higher than at SG at 25 m depth. Bacterial biomass was
370 comparable at both stations with higher biomass concentrations within the ice than in the water column. Bacterial activity
371 (based on DCF) was comparable in the bottom sea ice at the two sites; however, it was 63x higher in the brackish surface water
372 of SG leading to very high growth rate estimates (Table 2) of $6 \text{ mg C m}^{-3} \text{ d}^{-1}$. Due to a conversion factor from a very different
373 habitat (Molari et al., 2013), the absolute bacterial growth rate estimates are likely overestimations.

374 Integrated Chl values over the uppermost 25 m of the water column were nearly identical for SG and IE with values of about
375 $3.75 \text{ mg Chl m}^{-2}$ (Table 2). The fraction of Chl was highest at IE (85 %) and lowest at the SG (30 %) (Table 2). The integrated
376 NPP was considerably higher at SG ($42.6 \text{ mg C m}^{-2} \text{ d}^{-1}$ at SG, $0.2 \text{ mg C m}^{-2} \text{ d}^{-1}$ at IE), while the vertical export of Chl was
377 about three times higher at IE than SG. This leads to more (14 times) vertical export based on the sediment trap measurements
378 than production at IE and considerably lower (5 %) export than production at SG (Table 2). Relative to the standing stock
379 biomass of Chl at IE, 0.2 % of the Chl was renewed daily by NPP at IE and 3 % was vertically exported daily at IE, which
380 would relate - assuming absence of advection - to a daily loss of 3 % of the standing stock Chl. At SG, 38 % was renewed per
381 day, while 2 % were exported. As grazing was not estimated in this study, the suggested loss terms of Chl based on the sediment
382 trap data are likely underestimations. This leads to an accumulation of biomass of 38 % per day, and a doubling time of about
383 2.6 days. Bacterial growth doubling times were estimated to be between minutes (SG water) and days (IE water), but within
384 hours in sea ice (Table 2).

385 Considering the N demand based on the carbon based PP measurement ($16 \text{ mol C mol N}^{-1}$ after Redfield, 1934), about $2 \text{ } \mu\text{mol}$
386 $\text{N L}^{-1} \text{ month}^{-1}$ (equivalent to 32 % of 1 m value for NO_x) was needed to sustain the PP measured at SG. Assuming constant PP
387 and steady state nutrient conditions, 32 % of the surface water had to be replaced by subglacial upwelling per month to supply
388 this N demand via upwelling. Since only 62 % of the upwelling water was entrained bottom water the actual vertical water
389 replenishment rate would be 52 % per month. Assuming a 2 m freshwater layer under the ice, this translates to flux of about
390 $1.1 \text{ m}^3 \text{ m}^{-2} \text{ month}^{-1}$. Considering a distance of 250 m to the glacier front and a width of 1.6 km of the SG bay, this translates to
391 a minimum of about $422,000 \text{ m}^3 \text{ month}^{-1}$.

392 The reciprocal transplant experiment aimed to show the effect of water chemistry on primary production in the absence of
393 effects related to different communities, temperature, or light. The results (Fig. 7) showed clearly that the higher NPP at SG,

394 compared to NG was related to the nutrient concentrations (nested ANOVA, $p=0.0038$, $F=10.88$). In any combination, sterile
395 filtered water from the SG had a fertilising effect on both SG and IE communities, increasing PP of IE communities by approx.
396 30 %. SG communities of the most active fresh surface layer (1 m) fixed twice as much CO_2 when incubated in the same water,
397 compared to incubations in the IE water.

398 **3.4 Bacterial, archaeal and eukaryotic communities**

399 After bioinformatic processing 13,043 bacterial and archaeal (16S rRNA) OTUs, belonging to 1,208 genera with between
400 9,708 and 331,809 reads were retained. Differences between the bacterial 16S sequences of the various sample types indicated
401 that they can be used as potential markers for the origin of the water (Fig. 8). Sea ice and water communities are clearly
402 separated (ANOSIM, $p=0.004$, $R=0.35$) with no overlapping samples (Fig. 8a). Generally IE and NG communities were very
403 similar, while sea ice and under-ice water communities at SG were significantly different (ANOSIM, $p=0.001$, $R=0.593$) from
404 the other fjord samples. The NMDS showed also separation of 16S communities along a gradient from subglacial communities
405 towards fjord communities, with SG communities being in between fjord and subglacial communities (Fig. 8a). Bacterial
406 communities at SG in the bottom layer of the sea ice and the brackish water layer were more similar to subglacial outflow
407 communities than the other samples in both 2018 and 2019. Six OTUs were unique to the glacial outflow and SG surface
408 (closest relatives: *Fluviimonas*, *Corynebacterineae*, *Micrococcinae*, *Hymenobacter*, *Dolosigranuum*), which are 6.6 % of their
409 OTUs. The community structure of supraglacial ice was very different from any other sample. Also in the most abundant
410 genera clear differences can be detected (Fig. S1). *Flavobacterium* sp. was most abundant in sea ice and UIW samples in both
411 2018 and 2019 at SG, but rare or absent in the other samples. *Aliiglaciecola* sp. was characteristic for NG sea ice and UIW
412 samples. *Paraglaciecola* sp. was abundant in NG and IE sea ice and UIW samples, and *Colwellia* sp. was abundant in all sea
413 ice and UIW samples. In seawater samples the genus *Amphritea* sp. was more abundant. *Pelagibacter* sp. was abundant in all
414 samples. Glacial outflow water was dominated by *Sphingomonas* sp. and glacier ice by *Halomonas* sp., which were rare or
415 absent in the other samples.

416 The eukaryotic community (18S rRNA) consisted of 4,711 OTUs, belonging to 535 genera, with between 2,204 and 15,862
417 reads. Overall, the same NMDS clustering has been found as for the 16S rRNA sequencing. We found distinctive communities
418 in the sea ice and 1 m layer under the sea ice at SG being significantly different (ANOSIM, $p=0.001$, $R=0.456$) to the other
419 samples (Fig. 8c). In fact, the SG surface communities were more similar to the outflow community (Fig. 8c). The clear
420 differentiation between all sea ice and water column communities was also visible in the 18S rRNA samples (ANOSIM,
421 $p=0.005$, $R=0.192$). As for the 16S communities, also the abundant genera differed between the groups (Fig. S2). The
422 cryptophytes *Hemiselmis* sp. and Geminigeraceae were abundant at SG, but rare at the other sites. Dinophyceae, Imbricatea
423 (*Thaumatomastix* sp.) and Bacillariophyceae were abundant in all samples with diatoms being mostly more abundant in sea
424 ice or UIW. The Chytridiomycota family of Lobulomycetaceae were abundant in water samples from 2018, but not 2019.
425 Subglacial outflow water was dominated by unclassified Cercozoa and *Bodomorpha* sp..

426 In total 22 different taxa were detected by microscopy. The community composition was clearly separated between sea ice and
427 water samples. Furthermore sea ice species composition at SG differed from NG and IE (Fig. 8c). SG sea ice was completely
428 dominated by unidentified flagellates (potentially *Hemiselmis* sp., Geminigeraceae, and *Thaumatomastix* sp. based on 18S
429 sequences), with the exception of the 70–90 cm layer with high abundances of *Leptocylindrus minimus*. Sea ice samples at NG
430 and IE were dominated by the typical ice algae *Navicula* sp. and *Nitzschia frigida*. Water samples were more diverse with high
431 abundances of *Fragillariopsis* sp., *Coscinodiscus* sp., and *Chaetoceros* sp.. Overall, diatoms dominated most samples at NG
432 and IE in sea ice and water samples.

433 **4 Discussion**

434 The hydrography, sea ice properties, water chemistry and bacterial communities at SG provide clear evidence for submarine
435 discharge and upwelling at a shallow tidewater outlet glacier under sea ice, a system previously not considered for subglacial
436 upwelling processes. Briefly, our first hypothesis that submarine discharge persists also in early spring, supplying nutrient-
437 rich glacial meltwater and upwelling of bottom fjord water to the surface has been confirmed as discussed in detail below.

438 **4.1 Indications for submarine discharge and upwelling**

439 The physical properties at SG were distinctly different to stations NG and IE. In contrast to NG and IE, the marine terminating
440 SG site had a brackish surface water layer of 4 m thickness under the sea ice and low sea ice bulk salinities below 0.7 PSU,
441 with the exception of the uppermost 20 cm with a bulk salinity of 1.7 PSU. The sea ice bulk salinity is comparable to sea ice
442 in the nearby tidewater glacier influenced Tempelfjorden (Fransson et al., 2020) and brackish Baltic sea ice (Granskog et al.,
443 2003). We excluded surface melt or river runoff as freshwater sources for the following reasons. With air temperatures below
444 freezing point during the sampling periods, surface runoff based on snowmelt was not possible and no melting was observed
445 during fieldwork. In addition, there are no major rivers are known to flow into the main bay studied (Adolfbukta), due to the
446 small catchment areas (Norsk Polarinstitut, 2020). We did observe some subglacial runoff at the southern site of the glacier
447 (close to SG), but this outflow water froze before it reached the fjord, which was additionally blocked by a 1.33 m thick sea
448 ice cover. The sea ice cover would also block any inputs by atmospheric precipitation, considering the impermeable sea ice
449 conditions especially at SG with brine volume fractions below 5 % (Golden et al., 1998, Fransson et al., 2020). If surface
450 runoff was present, we would also expect a similar pattern at the NG site. In fact, due to the closer proximity to the southward
451 facing mountains and higher sea ice permeability, NG would be more likely influenced by surface runoff than SG. Other
452 potential freshwater sources could be related to terminus ice melt of glacier fronts, (Holmes et al., 2019, Sutherland et al.,
453 2019), icebergs (Moon et al., 2018), or ice melange (Mortensen et al., 2020). However, in the absence of Atlantic water inflow,
454 which is blocked by a shallow sill at the entrance of Billefjorden (Skogseth et al., 2020), water temperatures were consistently
455 below the freezing point (max -0.2 °C) and no Atlantic inflow water (Temperature ≥ 1 °C and Salinity ≥ 34.7 PSU, Skogseth
456 et al., 2020) was detected at any station. These low water temperatures do not allow glacier terminus ice to melt. Besides,

457 Billefjorden is not characterized by large amounts of icebergs or ice melange as described from Greenland glaciers (Moon et
458 al., 2018; Mortensen et al., 2020). However, glacier terminus ice melt is likely more important in systems with Atlantic water
459 inflows, such as Greenland or Svalbard fjords without a shallow sill (e.g. Kongsfjorden and Tunabreen, Holmes et al., 2019).
460 Sea ice may melt at lower temperatures compared to glacial ice, but the absence of typical sea ice algae in the water column
461 at SG and the low salinity of the sea ice indicated that this was not the case. In fact, sea ice with a salinity of 1.5 PSU (measured
462 at SG) would melt at $-0.08\text{ }^{\circ}\text{C}$ (Fofonoff et al., 1983), but the water and ice temperatures did not exceed $-0.2\text{ }^{\circ}\text{C}$. In fact, at this
463 temperature the brackish surface water and meltwater of the submarine discharge would be supercooled. We did find a 1.5 cm
464 layer of frazil ice on the bottom of the SG sea ice showing that this did have some influence on sea ice formation. The subglacial
465 meltwater would need to introduce some heat, allowing the meltwater to reach the surface as liquid water. A temperature
466 maximum at the sea ice-water interface supports this hypothesis. This heat may also lead to basal sea ice melt adding
467 freshwater closer to the glacier front and main plume. However, sea ice melt as freshwater source cannot explain the low
468 salinity of the sea ice itself. Consistent with our study Fransson et al. (2020) also found substantial amount of freshwater in
469 the sea ice in Tempelfjorden (approx. 50 % meteoric water fraction) in a year with large glacier meltwater contribution further
470 supporting the presence of submarine discharge under sea ice in our study. Fransson et al. (2020) suggested the combination
471 of low salinities with high silicate concentrations as indicator for glacial meltwater contributions, which was also the case in
472 our study. In addition, the overall low sea ice salinity and sediment inclusions at SG cannot be explained by sea ice melt, but
473 must originate from another source. Clear evidence for outflow comes also from the visual observations of subglacial outflow
474 exiting the land-terminating part south of the glacier in October 2019, April 2018 and April 2019, which we assume also
475 occurred under the marine terminating front. In fact, subglacial outflows in spring is a common phenomenon observed at
476 various other Svalbard glaciers with runoff originating from meltwater stored under the glacier from the last melt season and
477 released by changes in hydrostatic pressure or glacier movements (Wadham et al., 2001). Active subglacial drainage systems
478 in winter have also been described elsewhere, and can be sustained by geothermal heat or frictional dissipation, groundwater
479 inputs, or temperate ice in the upper glacier (Wilson 2012, Schoof et al., 2014). This meltwater has also been found to be rich
480 in silicate due to the long contact with the subglacial bedrock during its storage over winter (Wadham et al., 2001, Fransson et
481 al., 2020). We therefore suggest that early spring submarine discharge is not unique to Billefjorden, but likely occurs at all
482 polythermal or warm based marine-terminating glaciers.

483 **4.2 Potential magnitude of submarine discharge and upwelling**

484 Considering the slow tidal currents in our study area ($<22\text{ m}$ per 6 h tidal period, Kowalik et al., 2015) and wind mixing
485 blocked by sea ice, a potential source of the freshwater within Billefjorden may be meltwater introduced during the late summer
486 to fall melt season and remaining throughout winter. Hence, the question of how much subglacial meltwater reaches the surface
487 in what timeframe is important. We estimated that the surface water was most likely exchanged on time scales of days to
488 weeks. Even slow vertical mixing would be capable to erode the halocline in over six months since the last melt season. The
489 turbidity peak that we observed at the halocline would also settle out in a short time (weeks), if not replenished by fresh inputs

490 (Meslard et al., 2018). We determined vertical export flux to account for approximately 4% of the Chl standing stock at 25 m
491 (Table 2). Considering that glacial sediment settles typically much faster than phytoplankton due its higher density this suggests
492 that the turbidity peak would erode within days to weeks without fresh sediment inputs via upwelling (Meslard et al., 2018).
493 Furthermore, the inorganic nitrogen demand for the measured primary production would consume the present nutrients in a
494 few (approx. 2) months. Assuming steady state, the nutrient uptake by phytoplankton primary production would require an
495 upwelling driven water flux of at least $1.1 \text{ m}^3 \text{ m}^{-2} \text{ month}^{-1}$.

496 Microbial communities (16S rRNA and 18S rRNA) in SG UIW and sea ice were similar to the subglacial outflow water.
497 Bacterial communities (16S rRNA) at SG shared 6.6 % of their OTUs with subglacial outflow communities, which is twice as
498 much as NG and IE (3.6 %) shared with the outflow communities. Considering the estimated bacterial production and biomass
499 (Table 2) at SG the doubling time of the bacteria would be between 0.5 h and 7 h (Table 2). However, the use of a conversion
500 factor for biomass production based on sediment bacterial data is adding uncertainty to the estimation of the bacterial doubling
501 time. Estimates reported from Kongsfjorden in April are indeed longer (3-10 days, Iversen & Seuthe, 2010), as are other Arctic
502 bacterioplankton doubling time estimates ranging between 1.2 days (Rich et al., 1997), 2.8 days (de Kluijver et al., 2013) and
503 weeks (2 weeks, Rich et al., 1997, 1 week, Kirchman et al., 2005).

504 Based on the growth in the range of hours to days, the distinctive community at SG would have changed to a more marine
505 community on time scales of weeks, assuming only growth of marine OTUs at SG and settling out or grazing of inactive glacial
506 bacteria taxa. Thus, we suggest that the presence of shared OTUs between SG and the glacial outflow may indicate a continuous
507 supply of fresh inoculum to sustain these taxa.

508 The amount of discharge and upwelling was estimated using hydrographic data. In our study, three water masses were
509 distinguished; i) subglacial outflow (SGO) with low salinity (0 PSU) relatively high temperatures ($>0 \text{ }^\circ\text{C}$) and high silicate
510 concentrations (Cape et al., 2019), (ii) deep local Arctic water (DLAW) entrained from approx. 20 m with low temperatures ($-$
511 $1.7 \text{ }^\circ\text{C}$) high salinities (34.7 PSU) and high nutrient concentrations (Skogseth et al., 2020), and iii) surface local Arctic water
512 (SLAW) with the same temperature and salinity signature as the DLAW, but depleted in nutrients (Skogseth et al., 2020).
513 Nutrients were depleted in the UIW, but not at 15 m depth, showing that the nutricline was shallower than 15 m. Hence,
514 submarine discharge at a glacier terminus depth of 20 m would be sufficient to cause upwelling of nutrient rich DLAW to the
515 surface. In fact, our mixing calculations (Equations 1-6) estimate that 32 % of the SG water 1 m under the sea ice was derived
516 by SGO, which pulled 1.6 times as much ($53 \text{ \% DLAW} : 32 \text{ \% SGO} = \text{ratio of } 1.6$) DLAW with it during upwelling. Fransson
517 et al. (2020) found that 30-60 % of glacier-derived meltwater was incorporated in the bottom sea ice at the glacier front of
518 Tempelfjorden, which is comparable to our study, again indicating that early spring submarine discharge and the resulting
519 formation of sea ice with low porosity is a widespread process at marine terminating glacier fronts in Svalbard. Uncertainties
520 with these estimates may be related to sea ice melt as additional freshwater source, and to slightly different nutrient
521 concentrations directly in the SG submarine discharge compared to the sampled subglacial outflow at some distance.

522 **4.3 Importance of submarine discharge and upwelling under sea ice**

523 To our knowledge, our study provides currently the only available estimate of subglacial upwelling in early spring. Our study
524 suggests that subglacial upwelling in spring results in a small volume transport of only about $1.1 \text{ m}^3 \text{ m}^{-2} \text{ month}^{-1}$ (approx. 2 m^3
525 s^{-1}) in Billefjorden. This estimate is based on the flux of nutrient rich bottom water needed to maintain the measured primary
526 production assuming steady state conditions and is therefore a rough, but conservative estimate. Due to logistical limitations,
527 we could not sample the submarine outflow directly at the SG site, but at some distance. Consequently, submarine discharge
528 at SG may have slightly different nutrient concentrations due to potentially different bedrock chemistry. The most comparable
529 estimate on the magnitude of the upwelling is available at Kronebreen for summer. This Svalbard tidewater glacier is of similar
530 size and had one order of magnitude higher upwelling rates compared to our study ($31\text{-}127 \text{ m}^3 \text{ s}^{-1}$, Halbach et al., 2019). Due
531 to their size, summer subglacial upwelling flux in Greenland is two to four times higher than at Kronebreen ($250\text{-}500 \text{ m}^3 \text{ s}^{-1}$,
532 Carroll et al., 2016). In our study about 1.6 times as much bottom water from about 20 m (DLAW) as subglacial outflow water
533 (SOW) reached the surface at SG (Entrainment factor of 1.6 – see above). The entrainment factor is mostly dependent on the
534 depth of the glacier front (Carroll et al., 2016). In fact, the glacier terminus at SG was shallower (approx. 20 m) than any other
535 studied tidewater glacier on Svalbard (70 m depth at Kronebreen, Halbach et al., 2019) or Greenland ($> 100 \text{ m}$, Hopwood et
536 al., 2020). Hence, the higher summer entrainment factors estimated in Kongsfjorden (3, Halbach et al., 2019) and Greenland
537 (6 to 30, Hopwood et al., 2020) are not surprising. Glacier terminus depth appears to be the main control of entrainment rates,
538 likely independent of the time of the year. However, turbulent mixing may cause increased entrainment during times of very
539 high subglacial discharge rates. The higher entrainment factors in Greenland also lead to more saline water reaching the surface
540 and the strongly stratified brackish surface layer observed at SG has not been observed at these deep tidewater glaciers (e.g.
541 Mortensen et al., 2020). Kronebreen is the most comparable tidewater glacier in terms of glacier terminus depth and
542 entrainment rate. Although the estimated entrainment factor was low at Kronebreen (3), submarine upwelling substantially
543 increased summer primary production in Kongsfjorden (Halbach et al., 2019). In spite of the shallow depth, and the low
544 discharge and entrainment rate of our study, subglacial upwelling appears to be the main mechanism to replenish bottom water
545 with high nutrient concentrations to the surface and can substantially increase spring primary production due to; (i) submarine
546 outflow below (approx. 20 m) the nutricline ($<15 \text{ m}$), (ii) the absence of any other terrestrials inputs, (iii) Atlantic water blocked
547 by a shallow sill (Skogseth et al., 2020), (iv) very weak tidal currents (Kowalik et al., 2015), (iv) wind mixing blocked by sea
548 ice in Billefjorden, and (v) undiluted subglacial meltwater having lower nutrient concentrations than the DLAW.

549 **4.4 Importance for under-ice phytoplankton**

550 Our main finding was that i) higher irradiance, ii) a stratified surface layer, and iii) increased nutrient supply via subglacial
551 discharge and upwelling allowed increased phytoplankton primary production at SG. The ice edge station (IE) was light and
552 nutrient limited and supported a lower phytoplankton primary production.

553 **4.4.1 Increased light**

554 Despite the subglacial discharge and upwelling, the negative effect of light limitation with the massive sediment plumes in
555 summer (Pavlov et al., 2019) were not observed in early spring. We did measure a small turbidity peak under the SG sea ice,
556 but the values were comparable to open fjord systems in summer (Meslard et al., 2018, Pavlov et al., 2019), where light is
557 sufficient for photosynthesis. Under-ice phytoplankton blooms are typically limited by light, which is attenuated and reflected
558 by the snow and sea ice cover (Fortier et al., 2002, Mundy et al., 2009, Ardyna et al., 2020). Some blooms have been observed,
559 mostly under snow-free sea ice, such as after snow melt (Fortier et al., 2002), under melt ponds (Arrigo et al., 2012, Arrigo et
560 al., 2014), after rain events (Fortier et al., 2002), or at the ice edge related to wind-induced Ekman upwelling (Mundy et al.,
561 2009). In our study however, light levels available for phytoplankton growth were low compared to other under-ice
562 phytoplankton bloom studies (Mundy et al., 2009, Arrigo et al., 2012), but higher at SG than at IE. This can be explained
563 through the combined effects of sea ice and snow properties at SG. Light attenuation in low salinity sea ice is typically lower
564 due to a lower brine volume (Arst and Sipelgas, 2004). Also, lower sea ice algae biomass and thinner snow cover due to snow
565 removal with katabatic winds (e.g. Braaten 1997, Laska et al., 2012) leads to less light attenuation and a lower albedo. Our
566 estimates showed that about twice as much light reached the water at SG compared to the IE, in spite of the thicker sea ice
567 cover. The estimated light levels of 5 and 9 $\mu\text{E m}^{-2} \text{s}^{-1}$ were above the minimum irradiance ($1 \mu\text{E m}^{-2} \text{s}^{-1}$) required for primary
568 production (Mock & Gradinger, 1999). Hence, the increased light under the brackish sea ice at SG could be one factor
569 explaining the under-ice phytoplankton bloom observed.

570 **4.4.2 Stratified surface layer**

571 The strong stratification at SG is another factor; allowing phytoplankton to stay close to the surface, where light is available,
572 allowing a bloom to form. In fact, Lowry et al. (2017) found that convective mixing by brine expulsion in refreezing leads can
573 inhibit phytoplankton blooms even in areas with sufficient under-ice light and nutrients. At the same time, they found moderate
574 phytoplankton blooms under snow covered sea ice ($1\text{--}3 \text{ mg Chl m}^{-3}$) sustained by a more stratified surface layer, which was,
575 however, still an order of magnitude lower than the SG values. Our finding of a higher vertical flux at IE compared to SG
576 shows that stronger stratification may indeed be a contributing factor for the higher phytoplankton biomass at SG due to lower
577 loss rate. However, our reciprocal transplant experiment clearly showed, that location alone (light, stratification) could not
578 explain the increased primary production, but that the water properties at SG had a fertilising effect on algal growth, most
579 probable because of higher nutrient levels, which were limiting at IE. In contrast to SG, higher plume entrainment factors at
580 deep Greenland tidewater glaciers (Hopwood et al., 2020) lead to subglacial meltwater typically highly diluted with saline
581 bottom water, once it reaches the surface, resulting in high salinities and a rather weak salinity driven stratification directly at
582 the glacier front (Mortensen et al., 2020). Hence, the strong effect on stratification may be a unique feature of shallow tidewater
583 glaciers.

584 4.4.3 Upwelling and meltwater influx of nutrients

585 Algal growth at IE was co-limited by lower irradiance as well as nutrient concentrations. Dissolved inorganic nitrogen (DIN)
586 to phosphate ratios (N:P) at the IE were mostly below Redfield ratios (16:1), especially in sea ice with DIN concentrations
587 below $1 \mu\text{mol L}^{-1}$, indicating potential nitrogen limitations (Ptacnik et al., 2010), while the N:P ratio at SG was balanced and
588 close to Redfield. Silicate concentrations below $2 \mu\text{mol L}^{-1}$ are typically considered limiting for diatom growth (Egge &
589 Aksnes, 1992) and this threshold had been reached at UIW and sea ice (concentration estimate in brine volume) at IE, but not
590 at SG. This indicates that nitrate supplied by bottom water upwelling and silicate by combined upwelling and additions from
591 the glacial runoff had a fertilising effect on the SG water. High silicate values have also been observed at glacier fronts in other
592 areas such as Greenland fjords (Azetsu-Scott and Syvitski, 1997) and Tempelfjorden (Fransson et al., 2015:2020). Iron has not
593 been measured, but is an essential micronutrient, often enriched in subglacial meltwater (Bhatia et al., 2013, Hopwood et al.,
594 2020). However, iron limitation is untypical in coastal Arctic systems (Krisch et al., 2020). Besides the subglacial upwelling,
595 nutrient concentrations may simply be higher due to less physical forcing and time needed for vertical mixing down to the
596 bottom at the shallower water depth at SG compared to IE. However, NG was slightly shallower than SG and algal growth
597 was still limited by nutrients. Besides, silicate and nitrate showed negative correlations with salinity, when including SG
598 samples. In fact, these nutrients only correlated positively with salinity at IE and NG, while at SG, the negative correlations or
599 non-conservative mixing are indicative for subglacial upwelling (mainly N and Si) and/or meltwater input (for Si) (Hopwood
600 et al., 2020). Biological nutrient uptake did not play a significant role, due to relatively low bacterial and primary production.
601 The subglacial outflow water itself was poor in nitrate, but high in silicate due to the interaction with the subglacial bedrock
602 and long residence time below the glacier (Wadham et al., 2001), which was also found in Tempelfjorden (Fransson et al.,
603 2015, 2020). Nordenskiöldbreen has a mix of metamorphic bedrock including silicon rich gneiss, amphibolite, and quartzite,
604 but also carbonate rich marble (Strzelecki, 2011), which can partly contribute to the high silicate levels observed. The role of
605 bedrock derived minerals and particles for composition of sea ice chemistry have been described in the neighbouring fjord
606 (Tempelfjorden) in detail by Fransson et al. (2020). Silicate concentrations in subglacial outflow water were lower ($<1.5 - 2$
607 $\mu\text{mol L}^{-1}$) compared to estimates in Greenland (Meire et al., 2016a, Hawkings et al., 2017, Hatton et al., 2019), indicating that
608 direct fertilisation in early spring may be even more important in other tidewater glacier influenced fjords. Another potential
609 source may be higher silicate concentrations in the sediments at SG (Hawkings et al., 2017). While bottom water values were
610 similar between SG and IE, high concentrations in the SG sediments themselves is a probable source not accounted for in the
611 present study.

612 Another nitrogen source may be ammonium, which was introduced via subglacial upwelling in Kongsfjorden (Halbach et al.,
613 2019). Ammonium regeneration and subsequent nitrification (Christman et al., 2011) under the sea ice, may explain the
614 exceptionally high nitrate concentration of the UIW at SG, which can be part of the explanation for the high N:P ratios. In fact,
615 bacterial activity was higher at SG potentially allowing higher ammonium recycling. Another explanation for the high N:P
616 ratios and low phosphate concentrations can be related to phosphate scavenging by iron, as discussed by Cantoni et al. (2020).

617 Nitrate can be supplied through the subglacial meltwater itself (Wynn et al., 2007), but we did not find high nitrate
618 concentrations in the undiluted subglacial outflow water in our study. Atmospheric inputs of N have been shown in the Baltic
619 Sea, but thinner sea ice and warm periods with increased sea ice permeability were needed for the N to reach the brine pockets
620 or water column (Granskog et al., 2003). Our NO_x profiles show some evidence of atmospheric N deposition, but only at NG
621 and SG, which may be related to precipitation or surface flooding. For under-ice phytoplankton, these atmospheric N inputs
622 play probably no role, but may have benefitted the high *Leptocylindrus* algae biomass layer in the upper ice parts of SG.
623 Overall, the clearest evidence of nutrient limitations and fertilisation by submarine discharge and upwelling was demonstrated
624 with the reciprocal transplant experiment, which showed an approx. 30 % increase in primary production of algae communities
625 incubated in SG water. Overall, primary production at SG was an order of magnitude higher than at IE. This indicates that
626 both fertilisation by submarine discharge and upwelling and increased light and stratification play a role in increasing
627 phytoplankton primary production.

628 **4.4.4 Increased phytoplankton primary production**

629 The integrated primary production to 25 m at SG was 42.6 mg C m⁻² d⁻¹ which is low compared to other marine terminating
630 glacier influenced fjord systems in summer with integrated NPP of 480 ±403 mg C m⁻² d⁻¹ (Hopwood et al., 2020), including
631 studies in Kongsfjorden on Svalbard with 250 -900 mg C m⁻² d⁻¹ (Van de Poll et al., 2018). Also, studies conducted at the same
632 time (1 May) observed higher primary production rates in a marine-terminating glacier influenced fjord system, such as
633 Kongsfjorden (1520-1850 mg C m⁻² d⁻¹, Hodal et al., 2012). However, none of these systems were sea ice covered during the
634 study periods and therefore not limited by light compared to our study. Under sea ice, phytoplankton communities have
635 typically much lower NPP rates of 20–310 mg C m⁻² d⁻¹ with only about 10 % or less light transmission reaching the water
636 column (Mundy et al., 2009). These values are more comparable to the SG values, despite the lower estimated light
637 transmission (3 %). In the central Arctic, higher under-ice NPP has been measured, but always related to high light transmission
638 due to the absence of ice, or under melt ponds with light transmissions up to 59 % (Arrigo et al., 2012). However, in the sea
639 ice area north of Svalbard, Assmy et al. (2017) found substantial spring PP below relatively thick sea ice of refrozen leads.
640 This was also confirmed by a large CO₂ decrease due to primary production under the sea ice (Fransson et al., 2017).
641 Phytoplankton production under snow covered Arctic sea ice is often considered negligible compared to sea ice algae or
642 summer production. This can be shown in low biomass, mostly consisting of settling sea ice algae (Leu et al., 2015), or very
643 low NPP rates (e.g. Pabi et al., 2008). The same has been observed under Baltic sea ice with similar low light levels and
644 primary production between 0.1–5 mg C m⁻² d⁻¹ under snow covered sea ice and about 30 mg C m⁻² d⁻¹ under snow-free sea
645 ice (Haecky & Andersson, 1999). These values are comparable to the IE without subglacial meltwater influence, but an order
646 of magnitude lower than the production at SG. Moderate blooms of 1–3 mg Chl m⁻³ have been described under snow covered
647 sea ice with equal (3 %) light transmission (Lowry et al., 2017). Lowry et al. (2017) argues that a stratified water column and
648 sufficient nutrients allow moderate blooms even under these low light conditions. In particular, diatoms, the most common
649 taxa of under ice phytoplankton blooms (von Quillfeldt, 2000, this study) are known to be well adapted to low light conditions

650 (Furnas, 1990). Our study found Chl values up to an order of magnitude higher than Lowry et al. (2017), showing that under-
651 ice phytoplankton blooms are indeed important under snow covered sea ice and can be facilitated by submarine discharge and
652 upwelling.

653 Our study is the first to show that the combination of several factors (stratified water column, increased light and supply of
654 fresh nutrients via tidewater glacier driven processes) can support a rather productive under-ice phytoplankton community,
655 exceeding biomass and production of under-ice phytoplankton in systems with comparable light levels. Besides the increased
656 and extended primary production fuelled by tidewater glacier, the active and abundant phytoplankton taxa in surface water
657 with consistently replenished nutrients, may be a viable seed community for summer phytoplankton blooms, once the sea ice
658 disappears and light levels increase (Hegseth et al., 2019). The significantly different community at SG may also contribute to
659 an overall more diverse seed community available to the entire fjord, compared to fjords without early spring subglacial
660 discharge.

661 **4.5 Impact on sea ice algae**

662 **4.5.1 Impact on biomass and primary production**

663 While phytoplankton biomass and production were clearly increased at SG, exceeding levels of other snow covered under-ice
664 systems, sea ice algal biomass and activity had been differently affected. Our third hypothesis suggested lower sea ice algae
665 biomass and production at SG due to the lower brine volume fractions. In agreement with our hypothesis, algal biomass was
666 indeed an order of magnitude lower compared to the IE and NG. However, primary production was two times higher, showing
667 more efficient photosynthesis.

668 Compared to most other sea ice studies conducted during the same period of the year, typically representing the mid-bloom
669 phase with 10–20 mg Chl m⁻² (Leu et al., 2015), Chl biomass was very low at all stations of our study (<0.32 mg Chl m⁻²).
670 Only Greenland fjords (0.1-3.3 mg Chl m⁻²) or pre- and post-bloom systems had comparably low biomass (Mikkelsen et al.,
671 2008, Leu et al., 2015). The significantly different communities with a high number of cryptophyte flagellates, a high
672 proportion of phaeophytin (14–68 % in the bottom 3 cm), and a high contribution of sea ice algae in the water column indicate
673 that we sampled indeed a post-bloom situation. Considering the low air, sea ice and water temperatures and the absence of a
674 fresh UIW layer at the IE, the bloom was most likely not terminated by bottom ice erosion but by nutrient depletion. In fact,
675 SG bottom ice was deficient in phosphate (0.27 μmol (L brine)⁻¹), while IE was deficient in silicate (1 μmol (L brine)⁻¹) and
676 nitrogen (N:P = 1 mol N mol P⁻¹). This finding fits to earlier studies where phosphate limitations had been described as limiting
677 for brackish sea ice algae at concentrations below 0.27 μmol L⁻¹ (Haecky and Andersson, 1999), while N and Si limitations
678 are typical for Arctic sea ice algae (Gradinger, 2009). The low concentrations of phosphate in the subglacial meltwater would
679 partly explain the low concentration in SG sea ice. In addition, most studies summarized by Leu et al. (2015) were done 10
680 years or more prior to our measurements. In fact, the Greenland study by Mikkelsen et al. (2008) with comparable sea ice algae
681 biomass had the thinnest sea ice cover of 0.5 m sampled in the warmest year (2006). During our study, the weather station in

682 Longyearbyen measured a mean temperature of $-3.9\text{ }^{\circ}\text{C}$ in April 2019, which was $8.3\text{ }^{\circ}\text{C}$ above average and the second
683 warmest average April temperature recorded after April 2006 ($0.1\text{ }^{\circ}\text{C}$), indicating that a warmer climate may explain the earlier
684 bloom termination (yr.no).

685 Similar to algal biomass, primary production (approx. $0.01\text{ mg C m}^{-2}\text{ d}^{-1}$ at SG and $0.005\text{ mg C m}^{-2}\text{ d}^{-1}$ at IE, assuming 10 cm
686 productive bottom layer) was considerably lower than in most studies of Arctic sea ice ($0.8\text{--}55\text{ mg C m}^{-2}\text{ d}^{-1}$ in the Barents
687 Sea) mentioned by Leu et al.(2015). Only studies on algal aggregates (Assmy et al., 2013) and Baltic sea ice (Haecky &
688 Andersson, 1999) measured similarly low production rates indicating that the senescence of the bloom (aggregates) and brine
689 volume fraction (Baltic Sea) were factors contributing to low primary production in sea ice.

690 **4.5.2 Stressors in brackish sea ice**

691 In addition to the post bloom status of the bloom, the lower biomass at SG can be partly explained by the lower brine salinity.
692 Permeability of sea ice is typically related to salinity and temperature, which determine the brine volume. With a brine volume
693 fraction below 5 %, or a temperature below $-5\text{ }^{\circ}\text{C}$ and a salinity below 5 PSU, sea ice is considered impermeable (Golden et
694 al., 1998). At SG, temperatures were higher, but a brine volume fraction above 5 % was only found in bottom ice sections (7–
695 9 %), indicating that the brine channels are weakly connected and algae had limited inhabitable place and nutrient supply
696 (Granskog et al., 2003), especially in the upper layers of the sea ice. In more saline systems, such as the Chukchi or Beaufort
697 Sea a high flux of seawater through the ice ($0.4\text{--}19\text{ m}^3\text{ seawater m}^{-2}\text{ sea ice}$) has been discussed as crucial to allow continuous
698 primary production and accumulation of biomass (Gradinger, 2009). In impermeable ice, this flux is eliminated. However, the
699 algal biomass at SG was very low, even compared to other brackish sea ice system, such as the Baltic Sea with similar or lower
700 brine volume fractions and comparable light levels (Granskog et al., 2003: $3\text{--}6\text{ mg Chl m}^{-3}$, Haecky & Andersson, 1999: 1.2
701 mg Chl m^{-2}), indicating that other stressors played a role at SG. Grazing is assumed to be a minor control on algae production
702 and biomass in Arctic sea ice (Gradinger, 2002). However, grazing by heterotrophic flagellates on small primary producers
703 has been described as important in the Baltic Sea, indicating that it might play a role at SG as well (Haecky & Andersson,
704 1999). SG sea ice communities were indeed dominated by small flagellate algae (microscopy based) and a high proportion of
705 potential grazers (18S rRNA data). Other stressors, such as phosphate limitation, viral lysis, or osmotic stress related to episodic
706 outbursts of subglacial meltwater are likely additional factors explaining the low biomass.

707 DIC has also been described as potentially limiting for sea ice primary production, especially towards the end of the bloom
708 (Haecky & Andersson, 1999) and may be supplied with the carbonate rich subglacial outflow (Fransson et al., 2020). Higher
709 mortality due to factors mentioned above, together with the higher measured bacterial activity, allowing recycling of nutrients
710 may be a factor explaining higher production with lower Chl biomass. Lastly, nutrients may have been replenished recently
711 via advective processes when the brine volume fraction was higher.

712 At SG, another layer of potentially high activity has been found in the upper sea ice. In this layer, depleted nutrient
713 concentrations corresponded with high *Leptocylindrus minimus* abundances indicating that these algae were actively taking up
714 the nutrients, despite the impermeable sea ice. NO_x concentrations increased towards the surface and bottom indicating inputs

715 from surface flooding above (Granskog et al., 2003) and seawater below. Silicate and phosphate were only supplied from the
716 seawater below. The observed brine volume fractions below 5 % would not allow inputs of these nutrients, but episodes with
717 higher temperatures and thereby higher brine volume fractions may be sufficient to supply the needed nutrients to this
718 distinctive layer.

719 Overall, sea ice influenced by subglacial outflow was very similar to other brackish sea ice such as in the Baltic Sea concerning
720 structure, biomass and production (Haecky & Andersson, 1999, Granskog et al., 2005). Compared to Arctic sea ice sea ice
721 algae biomass was reduced due to low brine volume fractions, phosphate limitation and potentially higher mortality via grazing
722 and possibly higher osmotic stress.

723 **5 Outlook**

724 Our study showed that even a shallow marine-terminating glacier can lead to increased under-ice phytoplankton production
725 by locally enhanced light levels, stronger stratification and nutrient supply by submarine discharge and upwelling, which are
726 all factors expected to change due to climate change. While much of our evidence is circumstantial, the number of different
727 lines of evidence leading to the same conclusion makes our findings rather robust. We propose that our findings are applicable
728 to other shallow tidewater glaciers with a polythermal or warm base, as is common on Svalbard (Hagen et al., 1993, Irvine-
729 Fynn et al., 2011). In the shorter term, a longer melt season and presumably increased submarine discharge may lead to
730 increased subglacial upwelling in winter and spring. However, on longer time scales glaciers will retreat and transform towards
731 land terminating glaciers (Błaszczuk et al., 2009), which would result in the lack of submarine discharge and systems more
732 similar to the NG and IE with less nutrients and light available for phytoplankton. The local effect would reduce primary
733 production, biomass and bacterial production in the water column, but would result in higher biomass of sea ice algae with the
734 known Arctic taxa of pennate diatoms. Considering the increased sedimentation rate at IE, we expect the pelagic/sympagic
735 benthic coupling to become stronger supporting the benthic food web. Winter and spring submarine discharge is most likely
736 present at all polythermal or warm-based marine-terminating glaciers, which includes glacier termini with much deeper fronts,
737 much higher entrainment rates of bottom water, and higher silicate concentrations in the glacial meltwater (Hopwood et al.,
738 2020). Thus, the effect of early spring submarine discharge is likely more pronounced in other fjords. Additional effects of
739 climate change include increased precipitation in the Arctic, which would reduce light levels below the sea ice. However, also
740 land-terminating glaciers would allow snow removal by katabatic wind as discussed for Nordenskiöldbreen.

741 Another impact of climate change will be the reduction and earlier break-up of sea ice and Atlantification of fjords, leading to
742 increased light, and wind mixing. In the ice free Kongsfjorden, higher primary production rates have been measured in the
743 same month, indicating that the lack of sea ice may lead to increased overall primary production (Iversen & Seuthe, 2010).
744 However, Kongsfjorden is still influenced by subglacial upwelling, supplying nutrients for the bloom (Halbach et al., 2017).
745 In systems not affected by subglacial upwelling the additional light will most likely not lead to substantially higher primary
746 production as indicated by lower measured rates in these type of fjords (Hopwood et al., 2020). Since the entrainment in our
747 study occurs at only approximately 20 m depth, upwelling under sea ice-free conditions would have much less effect, since

748 wind induced mixing plays a more important role. Direct silicate fertilisation would also have less effect in an ice-free fjord
749 since the fjord is likely more nitrate than silicate limited, due to the later stage of the spring bloom (Hegseth et al., 2019). In
750 summary, we suggest that subglacial upwelling in early spring is important for phytoplankton blooms, but only in a sea-ice
751 covered fjord. The future of the spring phytoplankton blooms depends on what happens first, disappearance of sea ice, or
752 retreat of the glacier to land.

753 **6 Acknowledgements**

754 The field was funded by the individual Arctic field grants of the Svalbard Science forum for TV, UD, CD, and EH (project
755 numbers: 282622 (TV, UD, CD), 282600 (TV), 296538 (EH), 281806 (UD)). Additional, funding for lab work and analyses
756 was obtained by the ArcticSIZE - A research group on the productive Marginal Ice Zone at UiT (grant no. 01vm/h15). JE was
757 also supported by the the Ministry of Education, Youth and Sports of the Czech Republic ECOPOLARIS, project No.
758 CZ.02.1.01/0.0/0.0/16_013/0001708 and the Institute of Botany CAS (grant no. RVO 67985939). The publication charges for
759 this article have been partly funded by a grant from the publication fund of UiT The Arctic University of Norway.

760 We also wish to thank Jan Pechar, Jiří Štojd, and Marie Šabacká for field assistance; and Janne Søreide, Maja Hatlebekk,
761 Christian Zoelly, Marek Brož, Stuart Thomson, and Tore Haukås for field work preparation help. We are also acknowledged
762 to Melissa Brandner, Paul Dubourg, and Claire Mourgues for the help in the lab and Owen Wangensteen for the help with
763 bioinformatics analyses. We are thankful for the meteorological data of Petuniabukta supplied by Kamil Laska.

764 **7 Authors contributions**

765 TRV designed the experiments, formulated the hypotheses and developed the sampling design with contributions of CD and
766 UD, and RG. Fieldwork was conducted by TRV, UD, CD, EH, and JE with support by RG and EP for preparations. Lab
767 analyses were done by TRV, UD, EP, CD, MC and EH. Computational analyses were performed by TRV. The manuscript has
768 been prepared by TRV with contributions of all co-authors.

769 **8 Data availability**

770 Environmental data have been archived at Dataverse under the doi number <https://doi.org/10.18710/MTPR9E>. 18S and 16S
771 rRNA sequences have been archived at the European Nucleotide archive under the project accession number PRJEB40294.
772 The R and unix code for the statistical and bioinformatics analyses are available from the corresponding author upon request.
773 More detailed reports of the fieldwork are available in the Research in Svalbard database under the RiS-ID 10889.

774 **9 Competing interests**

775 The authors declare that they have no conflict of interest.

776 **References**

777 Ambrožová, K., and Láška, K.: Air temperature variability in the vertical profile over the coastal area of Petuniabukta, central
778 Spitsbergen, Polish Polar Research, 41-60, 2017.

779 Amundson, J. M., and Carroll, D.: Effect of topography on subglacial discharge and submarine melting during tidewater glacier
780 retreat, *Journal of Geophysical Research: Earth Surface*, 123(1), 66-79, 2018.

781 Ardyna, M., Mundy, C. J., Mills, M. M., Oziel, L., Grondin, P. L., Lacour, L., Verin, G., Van Dijken, G., Ras, J., Alou-Font,
782 E., Babin, M., Gosselin, M., Tremblay, J. É., Raimbault, P., Assmy, P., Nicolaus, M., Claustre, H. and Arrigo, K.R.:
783 Environmental drivers of under-ice phytoplankton bloom dynamics in the Arctic Ocean, *Elem Sci Anth*, 8(1), 30, DOI:
784 <http://doi.org/10.1525/elementa.430>, 2020.

785 Arrigo, K. R., Perovich, D. K., Pickart, R. S., Brown, Z. W., vanDijken, G. L., Lowry, K. E., Mills, M. M., Palmer, M. A.,
786 Balch, W. M., Bahr, F., Bates, N. R., Benitez-Nelson, C., Bowler, B., Brownlee, E., Ehn, J. K., Frey, K. E., Garley, R.,
787 Laney, S.R., Lubelczyk, L., Mathis, J., Matsuoka, A., Mitchell, G. B., Moore, G. W. K., Ortega-Retuerta, E., Pal, S.,
788 Polashenski, C.M., Reynolds, R. A., Schieber, B., Sosik, H. M., Stephens, M., P., and Swift, J. H.: Massive phytoplankton
789 blooms under Arctic sea ice, *Science*, 336, 1408, <https://org/10.1126/science.1215065>, 2012.

790 Arrigo, K. R., Arrigo, K. R., Perovich, D. K., Pickart, R. S., Brown, Z. W., van Dijken, G. L., Lowry, K. E., Mills, M. M.,
791 Palmer, M. A., Balch, W. M., Bates, N. R., Benitez-Nelson, C. R., Brownlee, E., Frey, K. E., Laney, S. R., Mathis, J., Matsuoka,
792 A., Mitchell, B. G., Moore, G. W. K., Reynolds, R. A., Sosik, H. A., Swift, J. H.: Phytoplankton blooms beneath the sea ice in
793 the Chukchi Sea, *Deep Sea Res. Part II Top. Stud. Oceanogr.*, 105, 1-16, <https://org/10.1016/j.dsr2.2014.03.018>, 2014.

794 Arst, H., and Sipelgas, L.: In situ and satellite investigations of optical properties of the ice cover in the Baltic Sea region, in:
795 *Proceedings of the Estonian Academy of Sciences, Biology and Ecology*, edited by: Aben, H., and Kurnitski, V., Estonian
796 Academy of Sciences, Tallinn, 25-36, 2004.

797 Assmy, P., Ehn, J. K., Fernández-Méndez, M., Hop, H., Katlein, C., Sundfjord, A., Bluhm, K., Daaase, M., Engel, A., Fransson,
798 A., Granskog, M. A., Hudson, S. R., Kristiansen, S., Nicolaus, M., Peeken, I., Renner, A. H. H., Spreen, G., Tatarek, A., and
799 Wiktor, J.: Floating ice-algal aggregates below melting Arctic sea ice, *PLoS ONE*, 8(10), e76599,
800 <https://org/10.1371/journal.pone.0076599>, 2013.

801 Assmy, P., M. Fernández-Méndez, P. Duarte, A. Meyer, A. Randelhoff, C. J. Mundy, L. M. Olsen, H. M. Kauko, A. Bailey, and
802 Chierici, M.: Leads in Arctic pack ice enable early phytoplankton blooms below snow-covered sea ice, *Scientific reports*, 7,
803 40850, 2017.

804 Atienza, S., Guardiola, M., Präbel, K., Antich, A., Turon, X., and Wangensteen, O. S.: DNA Metabarcoding of Deep-Sea
805 Sediment Communities Using COI: Community Assessment, Spatio-Temporal Patterns and Comparison with 18S rDNA,
806 Diversity, 12(4), 123, <https://org/10.3390/d12040123>, 2020.

807 Azetsu-Scott, K., and Syvitski, J. P. M.: Influence of melting icebergs on distribution, characteristics and transport of marine
808 particles in an East Greenland fjord, *Journal of Geophysical Research* 104 (C3), 5321–5328, 1999.

809 Bhatia, M. P., Kujawinski, E. B., Das, S. B., Breier, C. F., Henderson, P. B., and Charette, M. A.: Greenland meltwater as a
810 significant and potentially bioavailable source of iron to the ocean, *Nat Geosci*, 6(4), 274-278, <https://org/10.1038/ngeo1746>,
811 2013.

812 Błaszczyk, M., Jania, J. A., and Hagen, J. O.: Tidewater glaciers of Svalbard: Recent changes and estimates of calving fluxes,
813 *Pol Polar Res*, 2, 85-142, 2009.

814 Boyer, F., Mercier, C., Bonin, A., Le Bras, Y., Taberlet, P., and Coissac, E.: obitools: A unix-inspired software package for
815 DNA metabarcoding, *Mol Ecol Resour*, 16(1), 176-182, <https://org/10.1111/1755-0998.12428>, 2016.

816 Braaten, D. A.: A detailed assessment of snow accumulation in katabatic wind areas on the Ross Ice Shelf, Antarctica, *J*
817 *Geophys Res Atmos*, 102(D25), 30047-30058, <https://org/10.1029/97JD02337>, 1997.

818 Cantoni, C., Hopwood, M. J., Clarke, J. S., Chiggiato, J., Achterberg, E. P., and Cozzi, S.: Glacial drivers of marine
819 biogeochemistry indicate a future shift to more corrosive conditions in an Arctic fjord, *Journal of Geophysical Research:*
820 *Biogeosciences*, e2020JG005633, <https://doi.org/https://doi.org/10.1029/2020JG005633>, 2020.

821 Carroll, D., Sutherland, D. A., Hudson, B., Moon, T., Catania, G. A., Shroyer, E. L., Nash, J. D., Bartholomew, T. C., Felikson,
822 D., Stearns, L. A., Noël, B. P. Y., and van den Broeke, M. R.: The impact of glacier geometry on meltwater plume structure
823 and submarine melt in Greenland fjords, *Geophys. Res. Lett.*, 43, 9739–9748, <https://doi.org/10.1002/2016GL070170>, 2016.

824 Chandler, D. M., Wadham, J. L., Lis, G. P., Cowton, T., Sole, A., Bartholomew, I., Telling, J., Nienow, P., Bagshaw, E.B.,
825 Mair, D., Vinen, S., and Hubbard A.: Evolution of the subglacial drainage system beneath the Greenland Ice Sheet revealed
826 by tracers, *Nat Geosci*, 6(3), 195-198, <https://org/10.1038/ngeo1737>, 2013.

827 Christman, G. D., Cottrell, M. T., Popp, B. N., Gier, E., and Kirchman, D. L.: Abundance, diversity, and activity of ammonia-
828 oxidizing prokaryotes in the coastal Arctic Ocean in summer and winter, *Appl. Environ. Microbiol.*, 77(6), 2026-2034,
829 <https://org/10.1128/AEM.01907-10>, 2011

830 Cloern, J. E., Grenz, C., and Videgar-Lucas, L.: An empirical model of the phytoplankton chlorophyll: carbon ratio-the
831 conversion factor between productivity and growth rate, *Limnol. Oceanogr.*, 40(7), 1313-1321,
832 <https://org/10.4319/lo.1995.40.7.1313>, 1995.

833 Cox, G. F., and Weeks, W. F.: Equations for determining the gas and brine volumes in sea-ice samples, *J Glaciol*, 29(102),
834 306-316, <https://org/10.3189/S0022143000008364>, 1983.

835 De Kluijver, A., Soetaert, K., Czerny, J., Schulz, K. G., Boxhammer, T., Riebesell, U., and Middelburg, J. J.: A ¹³C labelling
836 study on carbon fluxes in Arctic plankton communities under elevated CO₂ levels, *Biogeosciences*, 10(3), 1425-1440, 2013.

837 Dickson, A. G., Sabine, C. L., and Christian, J. R.: Guide to best practices for ocean CO₂ measurements, PICES Special
838 Publication 3, 2007.

839 Dowdeswell, J. A.: On the nature of Svalbard icebergs, *J Glaciol*, 35(120), 224-234, <https://org/10.3189/S002214300000455X>,
840 1989.

841 Egge, J. K., and Aksnes, D.L.: Silicate as regulating nutrient in phytoplankton competition, *Mar Ecol Prog ser.* Oldendorf, 83,
842 281-289, <https://org/10.3354/meps083281>, 1992.

843 Esau, I., and Repina, I.: Wind climate in Kongsfjorden, Svalbard, and attribution of leading wind driving mechanisms through
844 turbulence-resolving simulations, *Advances in Meteorology*, <https://org/10.1155/2012/568454>, 2012.

845 Fransson, A., Chierci, M., Nomura, D., Granskog, M. A., Kristiansen, S., Martma, T., and Nehrke, G.: Influence of glacialwater
846 and carbonate minerals on wintertime sea-ice biogeochemistry and the CO₂ system in an Arctic fjord in Svalbard, *Annals of*
847 *Glaciology*, 1–21, <https://doi.org/10.1017/aog.2020.52>, 2020.

848 Fransson, A., Chierici, M., Skjelvan, I., Olsen, A., Assmy, P., Peterson, A., Spreen, G., and Ward, B.: Effect of sea-ice and
849 biogeochemical processes and storms on under-ice water fCO₂ during the winter-spring transition in the high Arctic Ocean:
850 implications for sea-air CO₂ fluxes, *J. Geophys. Res. Oceans*, 122, 5566–5587, doi: 10.1002/2016JC012478, 2017.

851 Fofonoff, P., and Millard R. C.: Algorithms for computation of fundamental properties of seawater, *Unesco Technical Papers*
852 *in Marine Science*, 44, 53, <http://hdl.handle.net/11329/109>, 1983.

853 Fortier, M., Fortier, L., Michel, C., and Legendre, L.: Climatic and biological forcing of the vertical flux of biogenic particles
854 under seasonal Arctic sea ice, *Mar. Ecol. Prog. Ser.*, 225, 1-16, <https://org/10.3354/meps225001>, 2002.

855 Furnas, M. J.: In situ growth rates of marine phytoplankton: approaches to measurement, community and species growth rate,
856 *J Plankton Res*, 12, 1117–1151, 1990.

857 Garrison, D. L., and Buck, K. R.: Organism losses during ice melting: a serious bias in sea ice community studies, *Polar Biol*
858 6:237-239, 1986.

859 Golden, K. M., Ackley, S. F., and Lytle, V. I.: The percolation phase transition in sea ice, *Science*, 282(5397), 2238-2241,
860 <https://org/10.1126/science.282.5397.2238>, 1998.

861 Gradinger, R.: Sea ice microorganisms, *Encyclopedia of environmental microbiology*, Wiley,
862 <https://org/10.1002/0471263397.env310>, 2003.

863 Gradinger, R.: Sea-ice algae: Major contributors to primary production and algal biomass in the Chukchi and Beaufort Seas
864 during May/June 2002, *Deep Sea Res. Part II Top. Stud. Oceanogr.*, 56(17), 1201-1212,
865 <https://org/10.1016/j.dsr2.2008.10.016>, 2009.

866 Granskog, M. A., Kaartokallio, H., and Shirasawa, K.: Nutrient status of Baltic Sea ice: Evidence for control by snow-ice
867 formation, ice permeability, and ice algae, *J Geophys Res Oceans*, 108(C8), <https://org/10.1029/2002JC001386>, 2003.

868 Guardiola, M., Uriz, M. J., Taberlet, P., Coissac, E., Wangenstein, O. S., and Turon, X.: Deep-sea, deep-sequencing:
869 metabarcoding extracellular DNA from sediments of marine canyons, *PloS one*, 10(10), e0139633, 2015.

870 Haecky, P., and Andersson, A.: Primary and bacterial production in sea ice in the northern Baltic Sea, *Aquat Microb Ecol*,
871 20(2), 107-118, <https://org/10.3354/ame020107>, 1999.

872 Hagen, J. O., Liestøl, O., Roland, E., and Jørgensen, T.: *Glacier Atlas of Svalbard and Jan Mayen*, Oslo: Norwegian Polar
873 Institute, 1993.

874 Halbach, L., Vihtakari, M., Duarte, P., Everett, A., Granskog, M. A., Hop, H., Kauko, H. M., Kristiansen, S., Myhre, P. I.,
875 Pavlov, A. K., Pramanik, A., Tatarek, A., Torsvik, T., Wiktor, J. M., Wold, A., Wulff, A., Steen, H., Assmy, P.: Tidewater
876 glaciers and bedrock characteristics control the phytoplankton growth environment in a fjord in the arctic, *Front Mar Sci*, 6,
877 254, <https://org/10.3389/fmars.2019.00254>, 2019.

878 Hatton, J. E., Hendry, K. R., Hawkings, J. R., Wadham, J. L., Kohler, T. J., Stibal, M., Beaton, A. D., Bagshaw, E. A., and
879 Telling, J.: Investigation of subglacial weathering under the Greenland Ice Sheet using silicon isotopes, *Geochim Cosmochim*
880 *Acta*, 247, 191-206, <https://org/10.1016/j.gca.2018.12.033>, 2019.

881 Hawkings, J. R., Wadham, J. L., Benning, L. G., Hendry, K. R., Tranter, M., Tedstone, A., Nienow, P., and Raiswell, R.: Ice
882 sheets as a missing source of silica to the polar oceans, *Nat. Commun*, 8(1), 1-10, <https://org/10.1038/ncomms14198>, 2017.

883 Hegseth, E. N., Assmy, P., Wiktor, J. M., Wiktor, J., Kristiansen, S., Leu, E., Tverberg, V., Gabrielsen, T. M., Skogseth, R.,
884 and Cottier, F.: Phytoplankton seasonal dynamics in Kongsfjorden, Svalbard and the adjacent shelf, in: *The Ecosystem of*
885 *Kongsfjorden, Svalbard*, edited by: Hop, H., and Wiencke, C., Springer, Cham., 173-227, 2019.

886 Hodal, H., Falk-Petersen, S., Hop, H., Kristiansen, S., and Reigstad, M.: Spring bloom dynamics in Kongsfjorden, Svalbard:
887 nutrients, phytoplankton, protozoans and primary production, *Polar Biol* 35, 191–203, [https://doi.org/10.1007/s00300-011-](https://doi.org/10.1007/s00300-011-1053-7)
888 [1053-7](https://doi.org/10.1007/s00300-011-1053-7), 2012.

889 Hodgkins, R.: Glacier hydrology in Svalbard, Norwegian high arctic, *Quat Sci Rev*, 16(9), 957-973, [https://org/10.1016/S0277-](https://org/10.1016/S0277-3791(97)00032-2)
890 [3791\(97\)00032-2](https://org/10.1016/S0277-3791(97)00032-2), 1997.

891 Holmes, F. A., Kirchner, N., Kuttenukeuler, J., Krützfeldt, J., and Noormets, R.: Relating ocean temperatures to frontal ablation
892 rates at Svalbard tidewater glaciers: Insights from glacier proximal datasets, *Sci. Rep*, 9(1), 1-11, [https://org/10.1038/s41598-](https://org/10.1038/s41598-019-45077-3)
893 [019-45077-3](https://org/10.1038/s41598-019-45077-3), 2019.

894 Hopwood, M. J., Carroll, D., Dunse, T., Hodson, A., Holding, J. M., Iriarte, J. L., Ribeiro, S., Achterberg, E. P., Cantoni, C.,
895 Carlson, D. F., Chierici, M., Clarke, J. S., Cozzi, S., Fransson, A., Juul-Pedersen, T., Winding, M. S. and Meire, L.: How does
896 glacier discharge affect marine biogeochemistry and primary production in the Arctic?, *Cryosphere*, 14, 1347-1383, [https://org/](https://org/10.5194/tc-14-1347-2020)
897 [10.5194/tc-14-1347-2020](https://org/10.5194/tc-14-1347-2020), 2020.

898 Irvine-Fynn, T. D., Hodson, A. J., Moorman, B. J., Vatne, G., & Hubbard, A. L.: Polythermal glacier hydrology: A review,
899 *Reviews of Geophysics*, 49(4), 2011.

900 Iversen, K. R., and Seuthe, L.: Seasonal microbial processes in a high-latitude fjord (Kongsfjorden, Svalbard): I. Heterotrophic
901 bacteria, picoplankton and nanoflagellates, *Polar Biol*, 34(5), 731-749, <https://org/10.1007/s00300-010-0929-2>, 2011.

902 Jones, E., Chierici, M., Skjelvan, I., Norli, M., Børsheim, K. Y., Lødemel, H. H., Sørensen, K., King, A. L., Lauvset, S.,
903 Jackson, K., de Lange, T., Johannessen, T., and Mourgues, C.: Monitoring ocean acidification in Norwegian seas in 2018,
904 Miljødirektoratet, M-1417|2019, 2019.

905 Kanna, N., Sugiyama, S., Ohashi, Y., Sakakibara, D., Fukamachi, Y., and Nomura, D.: Upwelling of macronutrients and
906 dissolved inorganic carbon by a subglacial freshwater driven plume in Bowdoin Fjord, northwestern Greenland, *J Geophys*
907 *Res Biogeosci*, 123(5), 1666-1682, <https://org/10.1029/2017JG004248>, 2018.

908 Kartverket, <https://kartkatalog.geonorge.no/metadata/kartverket/dybdedata/2751aacf-5472-4850-a208-3532a51c529a>, last
909 access: 10 August 2020.

910 Kirchman, D. L., Malmstrom, R. R., and Cottrell, M. T.: Control of bacterial growth by temperature and organic matter in the
911 Western Arctic, *Deep Sea Research Part II: Topical Studies in Oceanography*, 52(24-26), 3386-3395, 2005.

912 Kowalik, Z., Marchenko, A., Brazhnikov, D., and Marchenko, N.: Tidal currents in the western Svalbard Fjords, *Oceanologia*,
913 57(4), 318-327, <https://org/10.1016/j.oceano.2015.06.003>, 2015.

914 Krisch, S., Browning, T. J., Graeve, M., Ludwichowski, K.U., Lodeiro, P., Hopwood, M. J., Roig, S., Yong, J. C., Kanzow,
915 T., and Achterberg, E. P.: The Influence of Arctic Fe and Atlantic Fixed N on Summertime Primary Production in Fram Strait,
916 North Greenland Sea, *Sci. Rep.*, 10 (1), 15230, <https://doi.org/10.1038/s41598-020-72100-9>, 2020.

917 Leppäranta, M., and Manninen, T.: The brine and gas content of sea ice with attention to low salinities and high temperatures,
918 Finnish Institute of Marine Research Internal Report, 2, 1-15, 1988.

919 Láska, K., Witoszová, D., and Prošek, P.: Weather patterns of the coastal zone of Petuniabukta, central Spitsbergen in the
920 period 2008–2010, *Polish Polar Research*, 297-318, 2012.

921 Leu, E., Mundy, C. J., Assmy, P., Campbell, K., Gabrielsen, T. M., Gosselin, M., Juul-Pedersen, T., and Gradinger, R.: Arctic
922 spring awakening—Steering principles behind the phenology of vernal ice algal blooms, *Prog Oceanogr*, 139, 151-170,
923 <https://org/10.1016/j.pocean.2015.07.012>, 2015.

924 Lowry, K. E., Pickart, R. S., Selz, V., Mills, M. M., Pacini, A., Lewis, K. M., Joy-Warren, H., Nobre, C., van Dijken, G. L.,
925 Grondin, P., Ferland, J., and Arrigo, K. R.: Under-ice phytoplankton blooms inhibited by spring convective mixing in
926 refreezing leads, *J Geophys Res Oceans*, 123(1), 90-109, <https://org/10.1002/2016JC012575>, 2018.

927 Lydersen, C., Assmy, P., Falk-Petersen, S., Kohler, J., Kovacs, K. M., Reigstad, M., Stehen, H., Strøm, H., Sundfjord, A.,
928 Varpe, Ø., Walczowski, W., Weslawski, K. M., and Zajaczkowski, M.: The importance of tidewater glaciers for marine
929 mammals and seabirds in Svalbard, Norway, *J Marine Sys*, 129, 452-471, <https://org/10.1016/j.jmarsys.2013.09.006>, 2014.

930 Maes, S.: Polar cod population structure: connectivity in a changing ecosystem, Ph.D. thesis, KU Leuven, Leuven, Belgium,
931 2017.

932 Mahé, F., Rognes, T., Quince, C., de Vargas, C., and Dunthorn, M.: Swarm: robust and fast clustering method for amplicon-
933 based studies, *PeerJ*, 2, e593, <https://org/10.7717/peerj.593>, 2014

934 Massicotte, P., Bécu, G., Lambert-Girard, S., Leymarie, E., and Babin, M.: Estimating underwater light regime under spatially
935 heterogeneous sea ice in the Arctic, *Appl. Sci.*, 8(12), 2693, <https://org/10.3390/app8122693>, 2018.

936 Meire, L., Meire, P., Struyf, E., Krawczyk, D. W., Arendt, K. E., Yde, J. C., Juul Pedersen, T., Hopwood, M. J., Rysgaard, S.,
937 and Meysman, F. J. R.: High export of dissolved silica from the Greenland Ice Sheet, *Geophys. Res. Lett.*, 43, 9173–9182,
938 <https://doi.org/10.1002/2016GL070191>, 2016a.

939 Meire, L., Mortensen, J., Rysgaard, S., Bendtsen, J., Boone, W., Meire, P., and Meysman, F. J.: Spring bloom dynamics in a
940 subarctic fjord influenced by tidewater outlet glaciers (Godthåbsfjord, SW Greenland), *J Geophys Res Biogeosci*, 121(6),
941 1581-1592, <https://org/10.1002/2015JG003240>, 2016b.

942 Meslard, F., Bourrin, F., Many, G., and Kerhervé, P.: Suspended particle dynamics and fluxes in an Arctic fjord (Kongsfjorden,
943 Svalbard), *Estuarine, Estuar Coast Shelf S*, 204, 212-224, <https://org/10.1016/j.ecss.2018.02.020>, 2018.

944 Mortensen, J., Rysgaard, S., Bendtsen, J., Lennert, K., Kanzow, T., Lund, H., and Meire, L.: Subglacial Discharge and Its
945 Down-Fjord Transformation in West Greenland Fjords With an Ice Mélange, *J Geophys Res Oceans*, 125(9), e2020JC016301,
946 2020.

947 Moskalik, M., Cwiąkała, J., Szczuciński, W., Dominiczak, A., Głowacki, O., Wojtysiak, K., and Zagórski, P.: Spatiotemporal
948 changes in the concentration and composition of suspended particulate matter in front of Hansbreen, a tidewater glacier in
949 Svalbard, *Oceanologia*, 60(4), 446-463 2018.

950 Mock, T., and Gradinger, R.: Determination of Arctic ice algal production with a new in situ incubation technique, *Mar. Ecol.*
951 *Prog. Ser.*, 177, 15-26, <https://org/10.3354/meps177015>, 1999.

952 Molari, M., Manini, E., and Dell'Anno, A.: Dark inorganic carbon fixation sustains the functioning of benthic deep-sea
953 ecosystems, *Global Biogeochem Cycles*, 27(1), 212-221, <https://org/10.1002/gbc.20030>, 2013.

954 Moon, T., Sutherland, D. A., Carroll, D., Felikson, D., Kehrl, L., and Straneo, F.: Subsurface iceberg melt key to Greenland
955 fjord freshwater budget, *Nat Geosci*, 11(1), 49-54, <https://org/10.1038/s41561-017-0018-z>, 2018.

956 Mundy, C. J., Barber, D. G., and Michel, C.: Variability of snow and ice thermal, physical and optical properties pertinent to
957 sea ice algae biomass during spring, *J Marine Sys*, 58(3-4), 107-120, <https://org/10.1016/j.jmarsys.2005.07.003>, 2005.

958 Mundy, C. J., Gosselin, M., Ehn, J., Gratton, Y., Rossnagel, A., Barber, D. G., Martin, J., Tremblay, J., Palmer, M., Arrigo,
959 K. R., Darnis, G., Fortier, L., Else, B., Papakyriakou, T.: Contribution of under-ice primary production to an ice-edge upwelling
960 phytoplankton bloom in the Canadian Beaufort Sea, *Geophys. Res. Lett.*, 36(17), <https://org/10.1029/2009GL038837>, 2009.

961 Natural Earth, <http://www.natureearthdata.com/>, last access: 10 August 2020.

962 Norwegian Polar institute, Toposvalbard, <https://toposvalbard.npolar.no>, last access: 16 September 2020.

963 Pabi, S., van Dijken, G. L., and Arrigo, K. R.: Primary production in the Arctic Ocean, 1998–2006, *J Geophys Res Oceans*,
964 113(C8), <https://org/10.1029/2007JC004578>, 2008.

965 Parada, A. E., Needham, D. M., and Fuhrman, J. A.: Every base matters: assessing small subunit rRNA primers for marine
966 microbiomes with mock communities, time series and global field samples, *Environ. Microbiol.*, 18(5), 1403-1414,
967 <https://org/10.1111/1462-2920.13023>, 2016.

968 Parsons, T. R., Maita, Y. and Lalli, C. M. (Eds.): *A Manual of Chemical and Biological Methods for Seawater Analysis*.
969 Pergamon Press, Toronto, 1984.

970 Pavlov, A. K., Leu, E., Hanelt, D., Bartsch, I., Karsten, U., Hudson, S. R., Gallet, J., Cottier, F., Cohen, J. H., Berge, J.,
971 Johnsen, G., Maturilli, M., Kowalczyk, P., Sagan, S., Meler, J., and Granskog, M. A.: The underwater light climate in
972 Kongsfjorden and its ecological implications, in: *The Ecosystem of Kongsfjorden, Svalbard*, edited by: Hop, H., and Wiencke,
973 C., Springer, Cham., 137-170, 2019.

974 Perovich, D. K., Roesler, C. S., and Pegau, W. S.: Variability in Arctic sea ice optical properties, *J Geophys Res Oceans*,
975 103(C1), 1193-1208, <https://org/10.1029/97JC01614>, 1998.

976 Porter, K. G., and Feig, Y. S.: The use of DAPI for identifying and counting aquatic microflora, *Limnol Oceanogr*, 25, 943–
977 948, <https://wiley.com/10.4319/lo.1980.25.5.0943>, 1980.

978 Pruesse, E., Peplies, J., and Glöckner, F. O.: SINA: accurate high-throughput multiple sequence alignment of ribosomal RNA
979 genes, *Bioinformatics*, 28(14), 1823-1829, 2012.

980 Ptacnik, R., Andersen, T., and Tamminen, T.: Performance of the Redfield ratio and a family of nutrient limitation indicators
981 as thresholds for phytoplankton N vs. P limitation, *Ecosystems*, 13(8), 1201-1214, <https://org/10.1007/s10021-010-9380-z>,
982 2010.

983 Quast, C., Pruesse, E., Yilmaz, P., Gerken, J., Schweer, T., Yarza, P., Replies, J., and Glöckner, F. O.: The SILVA ribosomal
984 RNA gene database project: improved data processing and web-based tools. *Nucleic acids research*, 41(D1), D590-D596,
985 2012.

986 Redfield, A. C.: On the proportions of organic derivatives in sea water and their relation to the composition of plankton, In
987 *James Johnstone Memorial Volume*, 176–192. Liverpool University Press, 1934.

988 Rich, J., Gosselin, M., Sherr, E., Sherr, B., and Kirchman, D. L.: High bacterial production, uptake and concentrations of
989 dissolved organic matter in the Central Arctic Ocean, *Deep Sea Research Part II: Topical Studies in Oceanography*, 44(8),
990 1645-1663, 1997.

991 Sager, J. C., and Mc Farlane, J. C.: Radiation, in: *Plant growth chamber handbook*, edited by: Langhans, R. W., and Tibbits,
992 T. W., Iowa Agr. Home Econ. Expt. Sta. Special Rpt, 99, 1-29, 1997.

993 Schaffer, J., and Kanzow, T.: von Appen, W. J.; von Albedyll, L.; Arndt, J. E.; Roberts, D. H. Bathymetry Constrains Ocean
994 Heat Supply to Greenland’s Largest Glacier Tongue, *Nat. Geosci*, 13(3), 227-231, [https://doi.org/10.1038/s41561-019-0529-](https://doi.org/10.1038/s41561-019-0529-x)
995 [x](https://doi.org/10.1038/s41561-019-0529-x), 2020.

996 Schoof, C., Rada, C. A., Wilson, N. J., Flowers, G. E., and Haseloff, M.: Oscillatory subglacial drainage in the absence of
997 surface melt, *The Cryosphere*, 8(3), 959-976, 2014.

998 Skogseth, R., Olivier, L. L., Nilsen, F., Falck, E., Fraser, N., Tverberg, V., Ledang, A. B., Vader, A., Jonassen, M. O., Søreide,
999 J., Cottier, F., Berge, J., Ivanov, B. V., and Falk-Petersen, S.: Variability and decadal trends in the Isfjorden (Svalbard) ocean
1000 climate and circulation-an indicator for climate change in the European Arctic, *Prog Oceanogr*, 187, 102394,
1001 <https://org/10.1016/j.pocean.2020.102394>, 2020.

1002 Southwood, T. R. E. and Henderson, P. A. (Eds.): *Ecological methods*, John Wiley and Sons, 269, 2000.

1003 Strzelecki, M. C.: Schmidt hammer tests across a recently deglaciated rocky coastal zone in Spitsbergen—is there a "coastal
1004 amplification" of rock weathering in polar climates?, *Pol Polar Res*, 239-252, <https://org/10.2478/v10183-011-0017-5>, 2011.

1005 Sutherland, D. A., Pickart, R. S., Peter Jones, E., Azetsu-Scott, K., Jane Eert, A., and Ólafsson, J.: Freshwater composition of
1006 the waters off southeast Greenland and their link to the Arctic Ocean, *J Geophys Res Oceans*, 114(C5),
1007 <https://org/10.1029/2008JC004808>, 2009.

1008 Sutherland, D. A., Straneo, F., & Pickart, R. S.: Characteristics and dynamics of two major Greenland glacial fjords, *Journal*
1009 *of Geophysical Research: Oceans*, 119(6), 3767-3791, 2014.

1010 Thronsdon, J., Hasle, G. R., & Tangen, K. (Eds.): *Phytoplankton of Norwegian coastal waters*, Almatel Forlag AS, 2007.

1011 Tomas, C. R. (Ed.): *Identifying Marine Phytoplankton*, Elsevier, San Diego, 1997.

1012 Utermöhl, H.: Methods of collecting plankton for various purposes are discussed, *SIL Commun* 1953-1996. 9, 1–38,
1013 <https://doi.org/10.1080/05384680.1958.11904091>, 1958.

1014 Van De Poll, W. H.; Kulk, G.; Rozema, P. D.; Brussaard, C. P. D.; Visser, R. J. W.; Buma, A. G. J. Contrasting Glacial
1015 Meltwater Effects on Post-Bloom Phytoplankton on Temporal and Spatial Scales in Kongsfjorden, Spitsbergen, *Elementa*,
1016 <https://doi.org/10.1525/elementa.307>, 2018.

1017 Vihtakari, M.: *PlotSvalbard: PlotSvalbard - Plot research data from Svalbard on maps*. R package version 0.9.2,
1018 <https://github.com/MikkoVihtakari/PlotSvalbard>, 2020.

1019 von Quillfeldt, C. H.: Common diatom species in Arctic spring blooms: their distribution and abundance, *Bot Mar*, 43(6), 499-
1020 516, <https://org/10.1515/BOT.2000.050>, 2000.

1021 von Quillfeldt, C. H., Ambrose, W. G., and Clough, L. M.: High number of diatom species in first-year ice from the Chukchi
1022 Sea, *Polar Biol*, 26(12), 806-818, <https://org/10.1007/s00300-003-0549-1>, 2003.

1023 Vonnahme, T. R., Devetter, M., Žárský, J. D., Šabacká, M., and Elster, J.: Controls on microalgal community structures in
1024 cryoconite holes upon high Arctic glaciers, Svalbard, *Biogeosciences*, 13, 659-674, <https://org/10.5194/bg-13-659-2016>, 2016.

1025 Wadham, J. L., Hodgkins, R., Cooper, R. J., and Tranter, M.: Evidence for seasonal subglacial outburst events at a polythermal
1026 glacier, Finsterwalderbreen, Svalbard, *Hydrol. Process.*, 15(12), 2259-2280, <https://org/10.1002/hyp.178>, 2001.

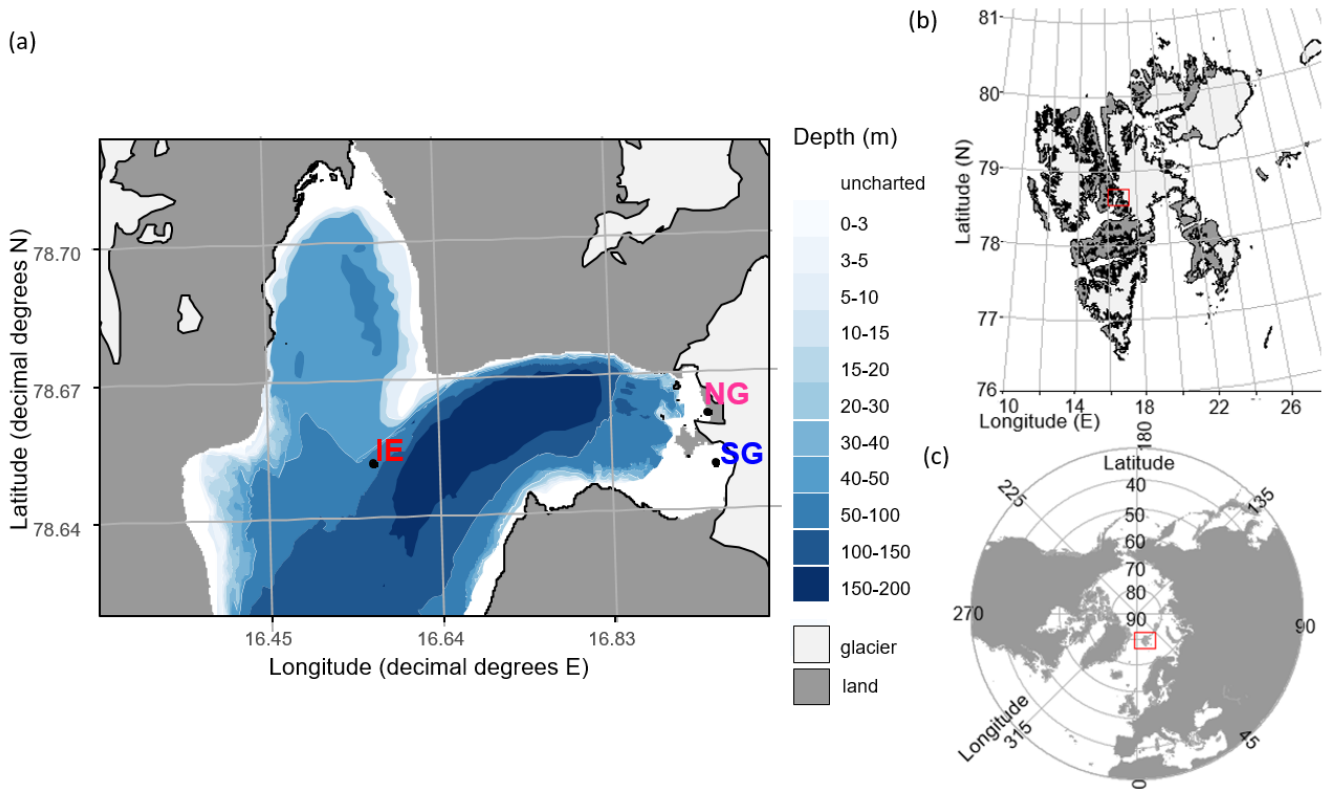
1027 Wang, Q., Garrity, G. M., Tiedje, J. M., and Cole, J. R.: Naive Bayesian Classifier for Rapid Assignment of rRNA Sequences
1028 into the New Bacterial Taxonomy, *Appl Environ Microbiol.* 73(16), 5261-7, <https://org/10.1128/AEM.00062-07>, 2007.

1029 Wangenstein, O. S., Palacín, C., Guardiola, M., and Turon, X.: DNA metabarcoding of littoral hard-bottom communities: high
1030 diversity and database gaps revealed by two molecular markers, *PeerJ*, 6, e4705, <https://org/10.7717/peerj.4705>, 2018.

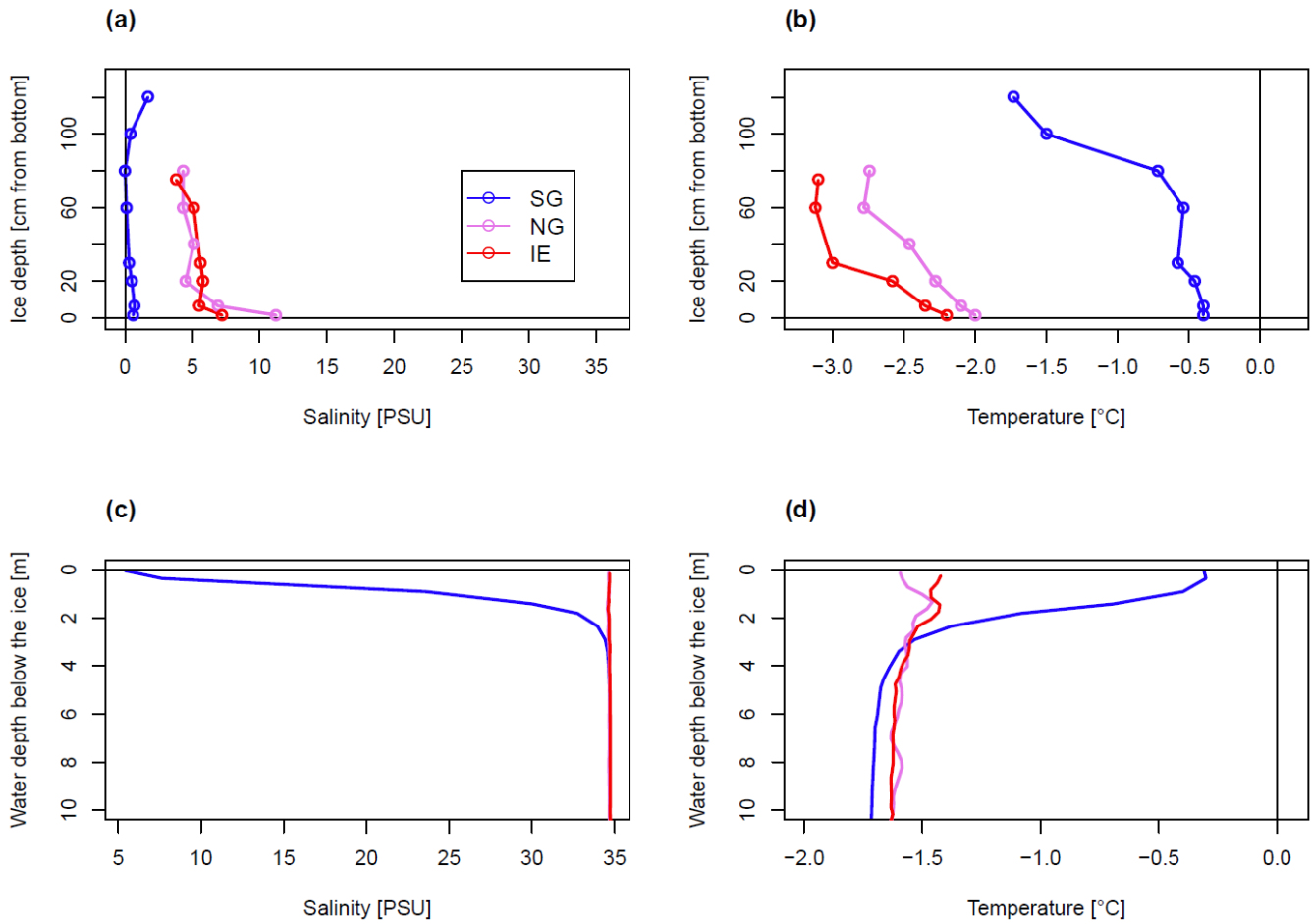
1031 Wiedmann, I., Reigstad, M., Marquardt, M., Vader, A., and Gabrielsen, T. M.: Seasonality of vertical flux and sinking particle
1032 characteristics in an ice-free high arctic fjord—Different from subarctic fjords?, *J Marine Sys*, 154, 192-205,
1033 <https://org/10.1016/j.jmarsys.2015.10.003>, 2016.

1034 Wilson, N.: Characterization and interpretation of polythermal structure in two subarctic glaciers, Doctoral dissertation,
1035 Science: Department of Earth Sciences, 2012.

1036 Wynn, P. M., Hodson, A. J., Heaton, T. H., and Chenery, S. R.: Nitrate production beneath a High Arctic glacier, Svalbard,
1037 Chemical geology, 244(1-2), 88-102, 2007.
1038 yr.no, Longyearbyen – historikk, [https://www.yr.no/nb/historikk/graf/1-](https://www.yr.no/nb/historikk/graf/1-2759929/Norge/Svalbard/Svalbard/Longyearbyen?q=2019-04)
1039 [2759929/Norge/Svalbard/Svalbard/Longyearbyen?q=2019-04](https://www.yr.no/nb/historikk/graf/1-2759929/Norge/Svalbard/Svalbard/Longyearbyen?q=2019-04), last access: 24 July 2020.
1040
1041
1042
1043
1044
1045
1046
1047
1048
1049
1050
1051
1052
1053
1054
1055
1056
1057
1058
1059
1060
1061
1062
1063
1064
1065
1066



1070 Fig 1. Sampling sites in Billefjorden: a) detailed Billefjorden map showing the stations at the ice edge (IE), north glacier (NG)
 1071 and south glacier (SG) on the underlying bathymetric map. White areas are uncharted with water depths of about 30 m at NG
 1072 and SG. The insets to the right show the location of b) Billefjorden on a Svalbard map and of c) Svalbard on a pan-Arctic map,
 1073 marked with red boxes. Land is shown as dark grey, ocean as white, and glaciers as light grey. All maps were created using
 1074 the PlotSvalbard R package (Vithakari, 2019). The Svalbard basemap is retrieved from the Norwegian Polar institute (2020,
 1075 CC BY 4.0 license), the pan-Arctic map is retrieved from Natural Earth (2020, CC Public domain license), and the bathymetric
 1076 map is retrieved from the Norwegian mapping authority (Kartverket, 2020, CC BY 4.0 license).



1080

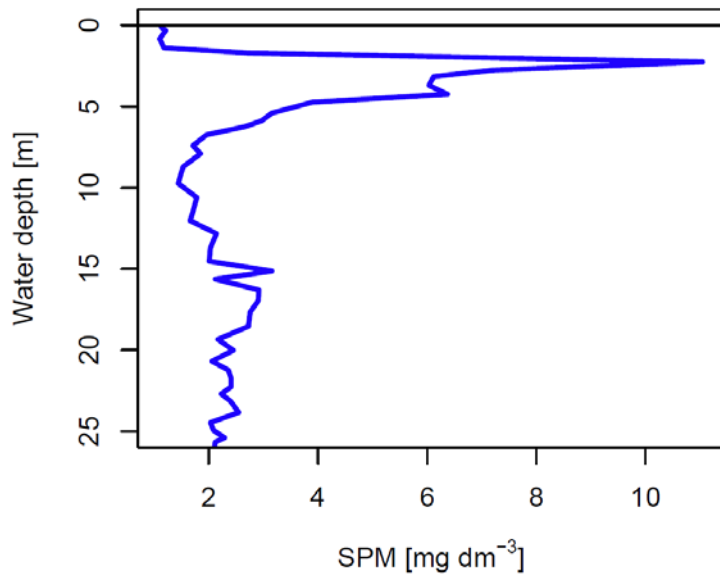
1081 Fig 2. Bulk salinity and temperature profiles in a,b) sea ice cores (0 cm at the bottom) and c,d) the water column down to 10
 1082 m below the sea ice, of the three stations.

1083

1084

1085

1086



1087

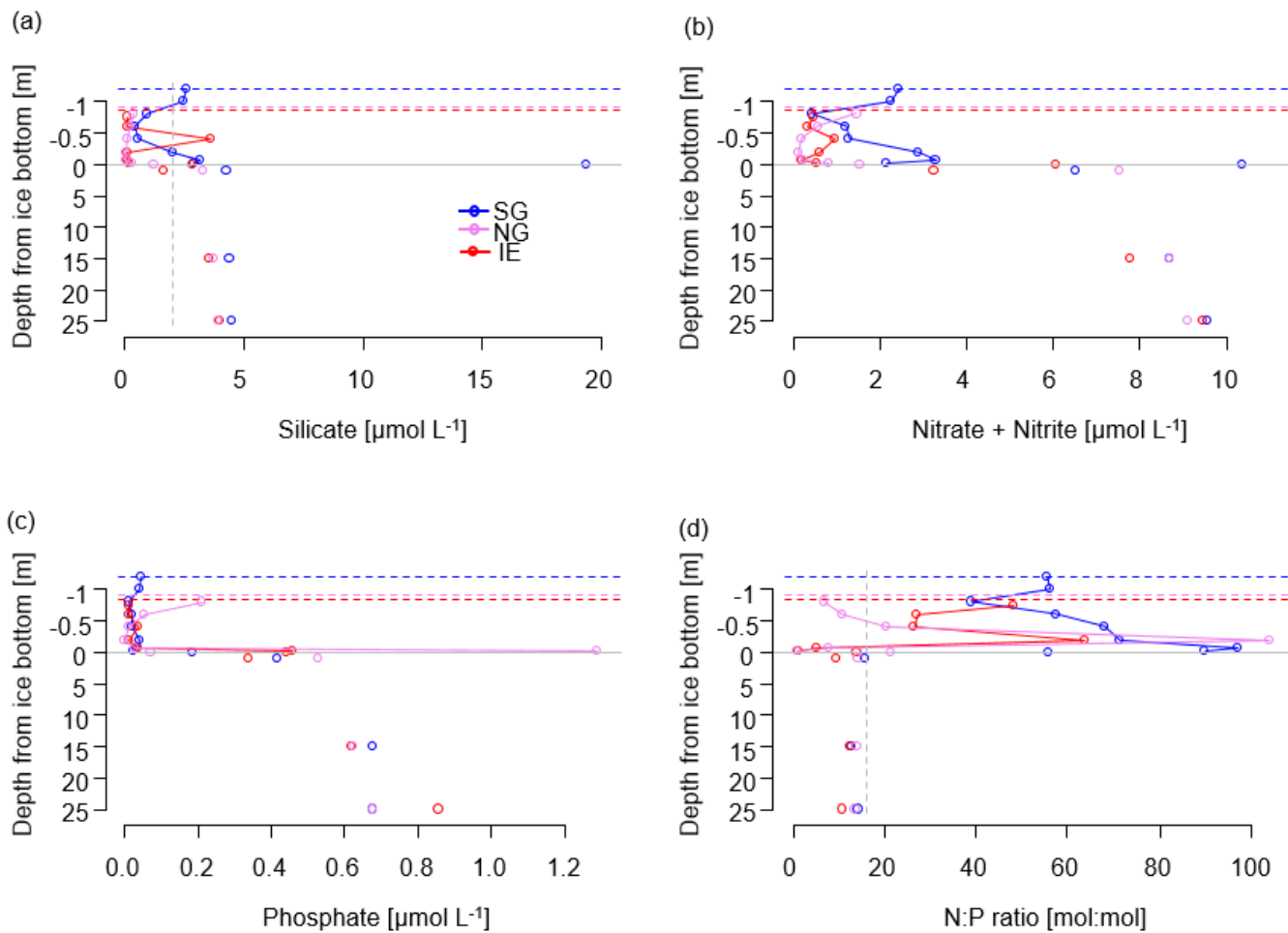
1088 Fig 3. Turbidity profile of the SG station converted to suspended particles.

1089

1090

1091

1092

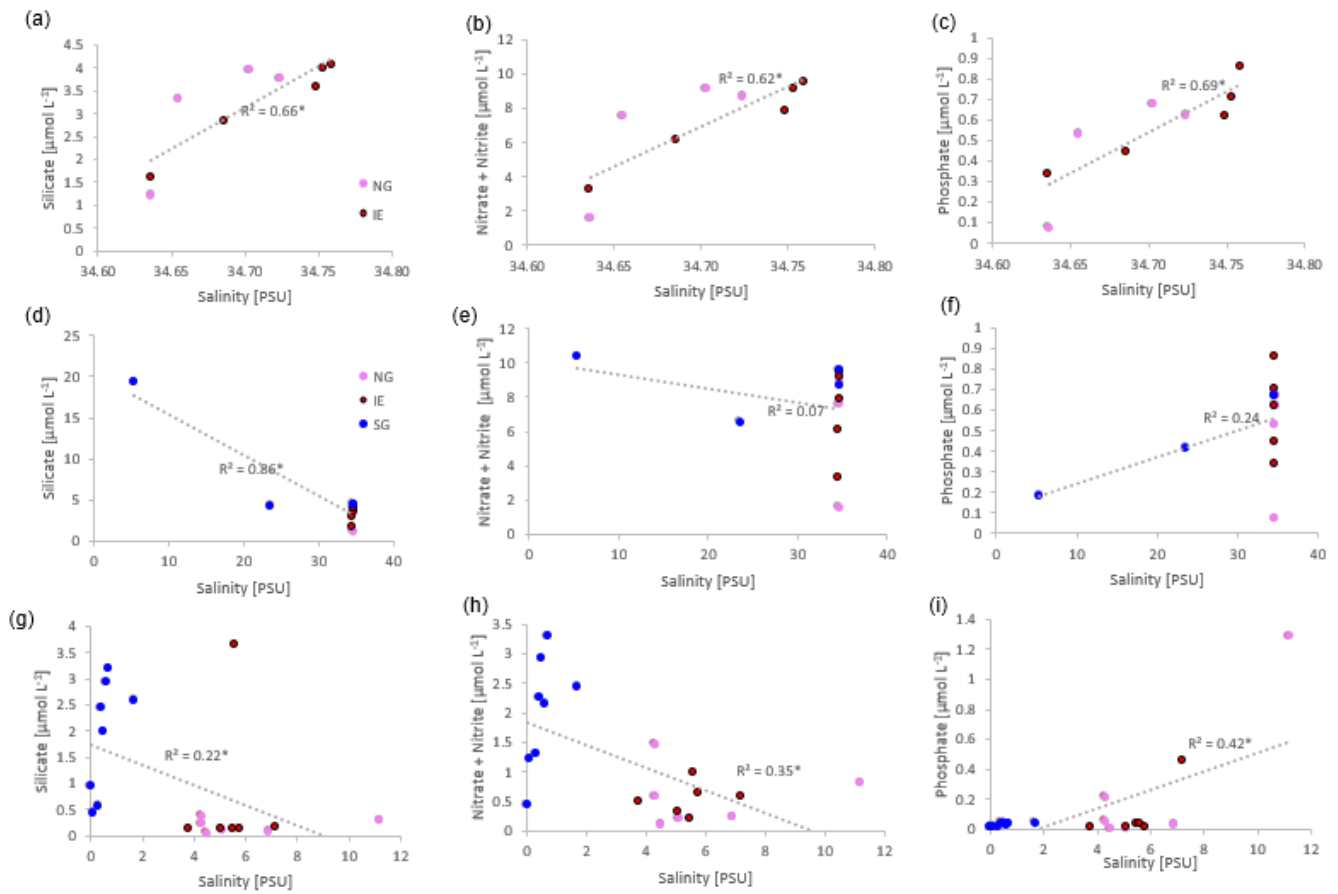


1093

1094 Fig 4. Nutrients in the water column (below grey line) and in sea ice (above the grey line) of a) silicate with a suggested
 1095 threshold for limitation marked as dashed grey line, b) NO_x as nitrate and nitrite, c) phosphate and d) molar N:P ratios with
 1096 the Redfield threshold of N:P 16:1 marked as dashed grey line indicating potential N limitation. Dashed lines indicate the
 1097 position of the ice surface, while solid lines show the measured data.

1098

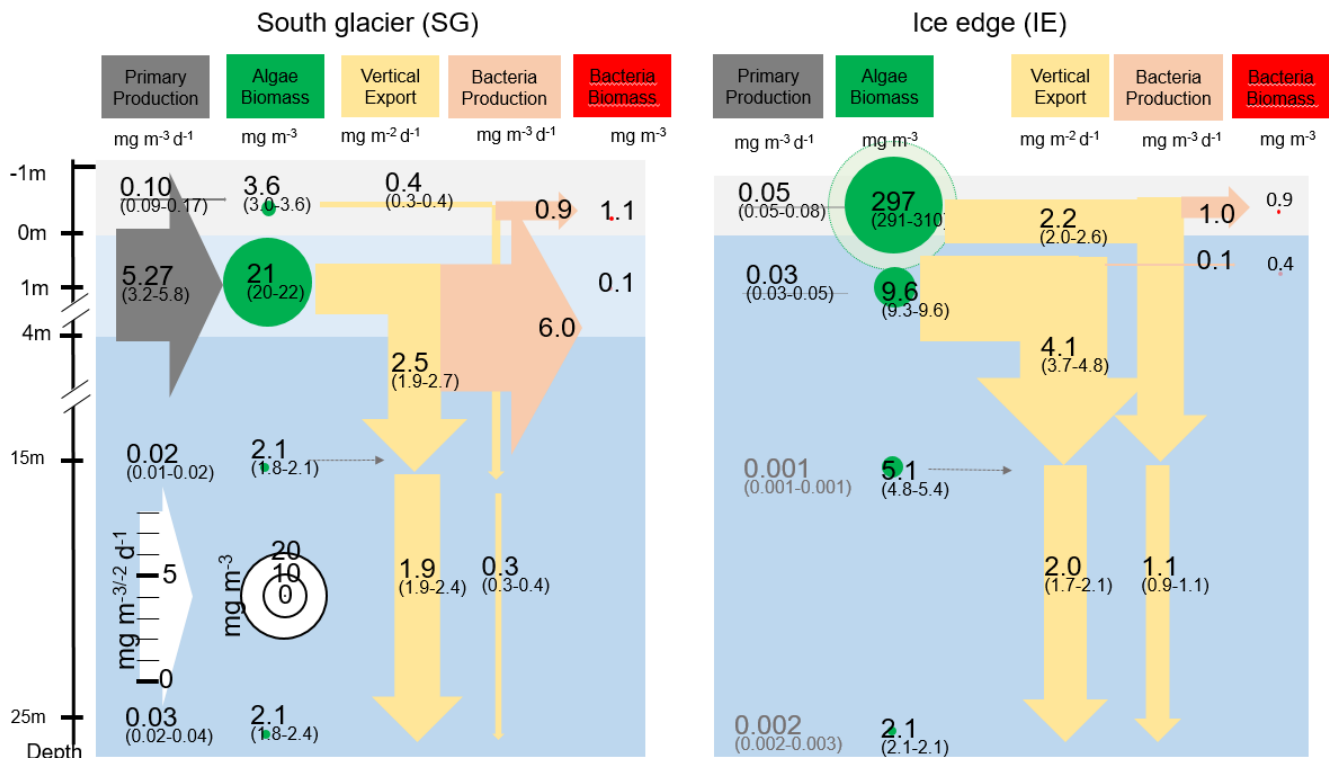
1099



1100

1101 Fig 5. Linear salinity-nutrient correlations of NG and IE water samples (a–c), NG, IE, and SG water stations (d–f) and sea ice
 1102 samples of NG, IE and SG (bulk salinities) (g–i). A higher concentration in saline Atlantic water is shown as a positive
 1103 correlation, a higher concentration in glacial meltwater as a negative correlation. Significant correlations ($p < 0.05$) are asterisk
 1104 marked behind the R^2 value.

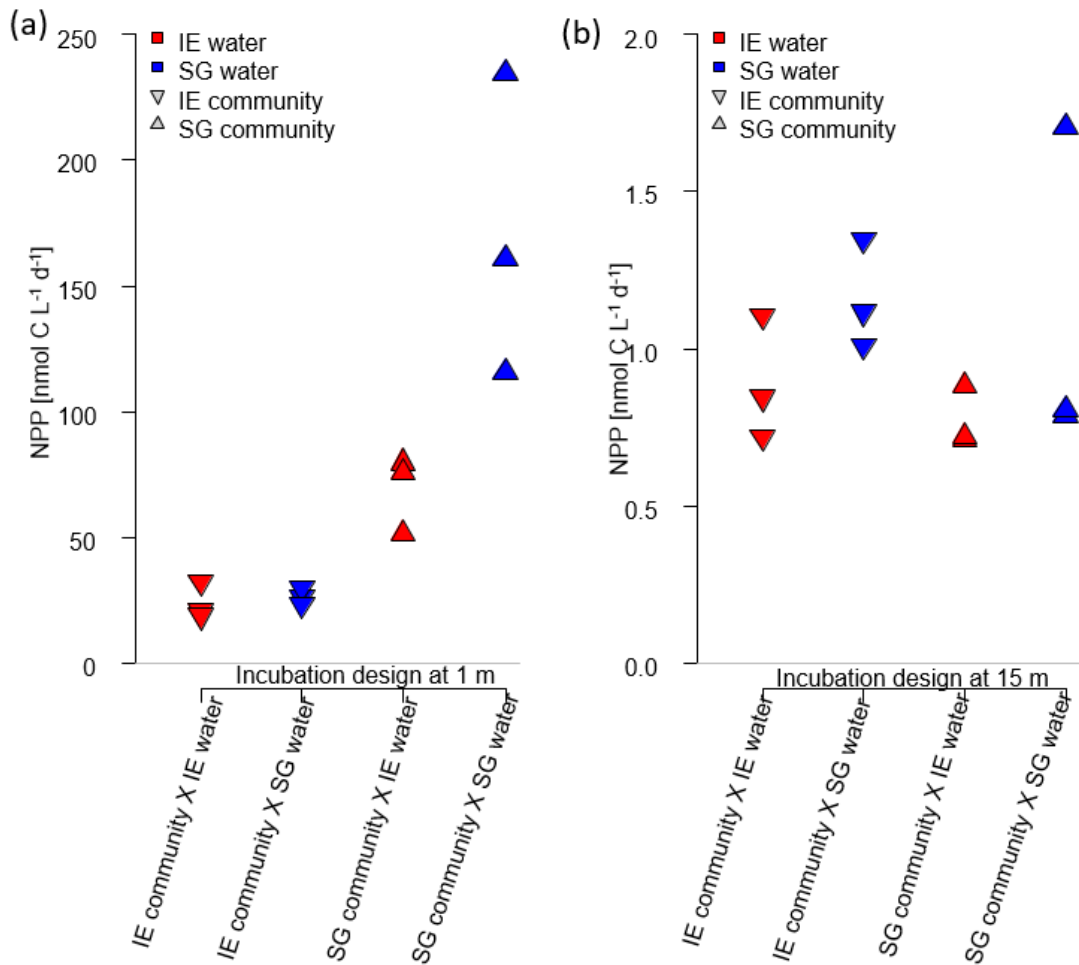
1105



1107

1108 Fig 6. Schematic representation of the C cycle at SG and IE stations. All units are in mg C with the median given in the circles
 1109 and arrows and the minimum and maximum in brackets below. 0 m depth is at the sea ice water interface. Grey arrows indicate
 1110 net primary production with its height scaled to the uptake rates. Green circles show standing stock algae biomass converted
 1111 from Chl to C (conversion factor = 30 gC gChl⁻¹, Cloern et al., 1995) with its diameter scaled to the concentrations, except sea
 1112 ice at IE with the light green circle scaled one order of magnitude higher. Yellow arrows indicate vertical export of chlorophyll
 1113 converted to C (conversion factor = 30 gC gChl⁻¹, Cloern et al., 1995) with the contribution of sea ice algae and phytoplankton
 1114 estimated by the fraction of typical sea ice algae in phytoplankton net hauls and the width of the arrows scaled to the fluxes.
 1115 Orange arrows indicate bacterial biomass production based on dark carbon fixation (conversion factor = 129 gC gDIC⁻¹, Molari
 1116 et al., 2013) with the arrows scaled to the values. Red circles to the right are bacteria biomass assuming 20 fg C cell⁻¹ in the
 1117 bottom sea ice and UIW. The grey area represents sea ice, the light blue area a brackish water layer and the darker blue area
 1118 deeper saline water layers.

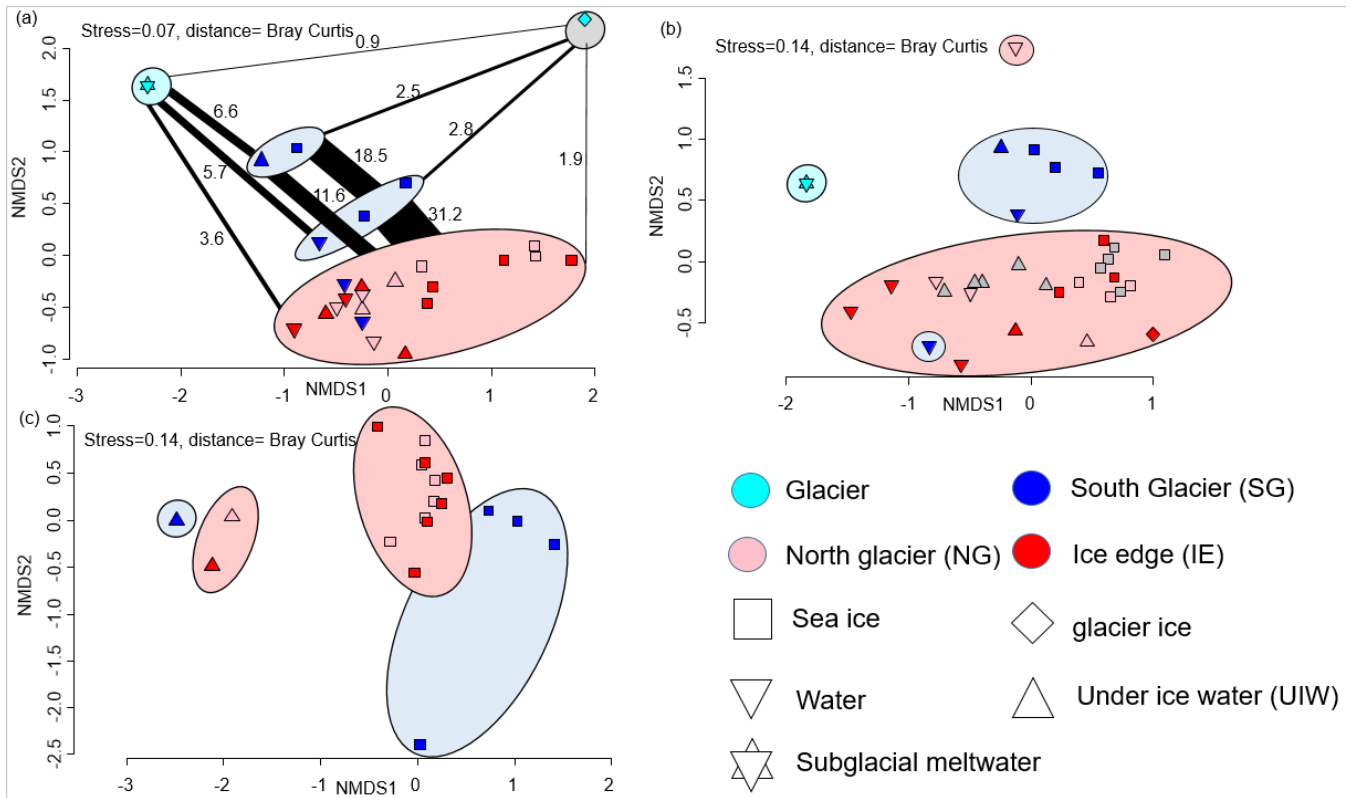
1119



1120

1121 Fig 7. Impact of water source on primary production assessed via a reciprocal transplant experiment. Primary production of
 1122 IE and SG communities incubated in sterile filtered water originated from either station at a) 1 m and b) 15 m depth. The
 1123 symbols show the source of the community and the colors indicate the source of the sterile filtered incubation water. The type
 1124 of incubation water (color) explains the variation in a nested ANOVA with community (symbol) and depth as nested
 1125 constrained variables and water source (color) as explanatory variable ($p=0.0038$, $F=10.88$).

1126



1128

1129 Fig 8. a) NMDS plot of microbial community structure based on 16S data (stress = 0.07), including samples from April 2018.
 1130 Groups highlighted in eclipses: glacier ice (top right in grey eclipse), undiluted subglacial outflow (top left in cyan eclipse),
 1131 surface samples (UIW, sea ice) at station SG 2019 (top blue eclipse), surface samples (1m water, sea ice) at station SG 2018
 1132 (bottom blue eclipse) and others including deeper water samples at SG (bottom in red eclipse). The fraction of shared OTUs
 1133 (in %) are shown as lines scaled to the fraction [%] of shared OTUs. b) NMDS plot of community structure based on 18S data
 1134 (stress = 0.14), including samples from April 2018 with the surface water sample of NG as outlier on top, and a surface water
 1135 sample of SG as outlier in the pink reference cluster, c) NMDS plot based on algae abundances in sea ice and UIW based on
 1136 light microscopic counts (stress = 0.14).

1137

1138

1139

1140

1141

1142

1143

1144 **Tables**

1145 Table 1. Properties of 1) marine surface and 2) Marine deep water (both station IE), 3) subglacial discharge melt water and 4)
 1146 station SG surface water and the relative contribution of the water types 1 to 3 to form water type 4. The calculations are given
 1147 in the Supplement and are based on different salinities and nutrients in the 4 water masses.

	1) Surface water (IE 1 m)		2) Bottom water (IE)		3) Subglacial discharge Meltwater		4) SG (1 m)
Salinity [PSU]	34.7		34.7		0 32 ± 0.1 %		23.6
Temperature [°C]	-1.4		-1.4		0		-0.4
Silicate [$\mu\text{mol L}^{-1}$]	1.59	0 %	4.46	> 84 %	1.79	32 %	4.30
NO _x [$\mu\text{mol L}^{-1}$]	3.27	10 ± 3 %	9.57	58 ± 1 %	2.06	32 %	6.52
Phosphate [$\mu\text{mol L}^{-1}$]	0.34	19 ± 3 %	0.67	49 ± 3 %	0.09	32 %	0.42

1148

1149

1150

1151

1152

1153

1154

1155

1156

1157

1158

1159

1160

1161

1162

1163

1164

1165

1166

1167

1168

1169 Table 2. Integrated standing stock biomass of Chl and fluxes of Chl and C, fractions of the different fluxes and standing stocks,
 1170 and bacterial production based on dark carbon fixation (DCF).

Variable	SG	IE	Unit
Chl integrated in sea ice	0.02	0.40	mg m ⁻²
NPP in bottom sea ice	0.10	0.05	mg C m ⁻³ d ⁻¹
Chl integrated in 25 m water column	3.74	3.75	mg m ⁻²
Vertical Chl flux to 25 m	0.07	0.11	mg Chl m ⁻² d ⁻¹
NPP at 1 m	5.27	0.03	mg C m ⁻³ d ⁻¹
C based NPP int. over 25 m	42.6	0.2	mg C m ⁻² d ⁻¹
Estimated Chl production int. over 25 m	1.4	0.0	mg C m ⁻² d ⁻¹
mg C fixed per mg Chl	11.4	0.1	mg C mg Chl d ⁻¹
NPP as fraction of Chl standing stock	38 %	0.2 %	% Chl renewal d ⁻¹
Doubling time	2.63	500	days
Vertical Chl flux as % of Chl standing stock	2 %	3 %	% export of Chl d ⁻¹
Vertical Chl flux as % of NPP based Chl prod.	5 %	1375 %	% export of NPP d ⁻¹
Loss of Chl from 15 to 25 m	12 %	19 %	Δexp 15m to 25m
Average Chl fraction of (Chl + Phaeo) in 0-3 cm ice	30%	85%	% Chl
Average Chl fraction of (Chl + Phaeo) in water	47 %	50 %	% Chl
Bacteria DCF ice	7.0	7.6	μg C m ⁻³ d ⁻¹
Bacteria Biomass prod (DCF based) ice	0.9	1.0	mg C m ⁻³ d ⁻¹
Doubling time	1.2	0.9	days
Bacteria DCF 1 m	46.9	1.1	μg DIC m ⁻³ d ⁻¹
Bacteria Biomass prod (DCF based) 1m	6.0	0.1	mg C m ⁻³ d ⁻¹
Doubling time	0.02	2.9	days

1171

1172

1173

1174

1175

1176

1177

1178

1179

1180 **Appendix**

1181 Equations 1-6. Mixing calculations for estimates of the fraction of meltwater (MW_{Sal}) based on salinity, and for bottom water
 1182 based on nutrient concentrations (BW_{Nuts}). Sal indicates the average salinities measured at the IE (Sal_{IE}), SG at 1m depth
 1183 (Sal_{SG1m}), subglacial outflow (Sal_{glac}). Nut indicates the nutrient concentrations of nitrate and nitrite (NO_x), silicate (Si), and
 1184 phosphate (PO_4) at 1m under the sea ice at SG (Nut_{1mSG}) and IE (Nut_{1mIE}), the bottom water of the IE (Nut_{BW}), or subglacial
 1185 outflow water (Nut_{glac}).
 1186

$$1187 \quad MW_{Sal}[\%] = \frac{Sal_{IE} - Sal_{SG1m}}{Sal_{SG1m} - Sal_{glac} + Sal_{IE} - Sal_{SG1m}} * 100 \quad (1)$$

$$1188 \quad MW_{Sal}[\%] = \frac{34.7 \text{ PSU} - 23.6 \text{ PSU}}{23.6 \text{ PSU} - 0 \text{ PSU} + 34.7 \text{ PSU} - 23.6 \text{ PSU}} * 100 = 32 \% \quad (2)$$

$$1189 \quad BW_{Nut}[\%] = \frac{Nut_{1mSG} - MW_{Sal}[\%] * Nut_{glac} - Nut_{1mIE} + MW_{Sal}[\%] * Nut_{1mIE}}{Nut_{BW} - Nut_{1mIE}} * 100 \quad (3)$$

$$1192 \quad BW_{NOx}[\%] = \frac{6.52 \mu M - 0.32 * 2.06 \mu M - 3.27 \mu M + 0.32 * 3.27 \mu M}{9.57 \mu M - 3.27 \mu M} * 100 = 58 \% \quad (4)$$

$$1194 \quad BW_{Si}[\%] = \frac{4.30 \mu M - 0.32 * 1.79 \mu M - 1.59 \mu M + 0.32 * 1.59 \mu M}{4.46 \mu M - 1.59 \mu M} * 100 = 92 \% \quad (5)$$

$$1196 \quad BW_{PO4}[\%] = \frac{0.41 \mu M - 0.32 * 0.09 \mu M - 0.34 \mu M + 0.32 * 0.34 \mu M}{0.67 \mu M - 0.34 \mu M} * 100 = 46 \% \quad (6)$$

1198 Equation 7. Calculation of vertical flux of Chl based on the sediment traps with concentration of Chl (C), Volume in the
 1199 sediment trap cylinder (V), area above the cylinder (A) and incubation time (t).

$$1200 \quad \text{Vertical flux} = \frac{C * V}{A * t} \quad (7)$$

1201
1202
1203
1204
1205
1206
1207
1208
1209
1210
1211
1212